

ULTRAFAST SPECTROSCOPY

MARCOS DANTUS AND PETER GROSS, *Department of Chemistry, Michigan State University, East Lansing, Michigan, U.S.A.*

	Introduction	431	4.1	Unimolecular	
1.	Physical Framework and			Photodissociation along a	
	Examples	432		Single Reaction Coordinate ..	445
1.1	Illustrative Example	435	4.2	Unimolecular	
1.2	Applications	436		Photodissociation along	
2.	Experimental Techniques			Multiple Reaction	
	and Methods	439		Coordinates	445
2.1	Ultrafast Laser Systems	439	4.3	Other Unimolecular	
2.2	Detection in Ultrafast			Reactions	446
	Spectroscopy: The Pump-		4.4	Bimolecular Reactions	448
	Probe Method	440	5.	Other Applications of	
3.	Ultrafast Spectroscopy of			Ultrafast Spectroscopy	449
	Molecules	440	5.1	Liquids	450
	Ultrafast Rotational		5.2	Solids	453
	Spectroscopy	441	5.3	Biological	453
3.2	Ultrafast Vibrational			Glossary	454
	Spectroscopy	443		Works Cited	455
3.3	Coherence and Dephasing	444		Further Reading	456
4.	Chemical Reactions	445			

INTRODUCTION

Spectroscopy in general is the study of the interaction between light and matter. It is the major tool used for the determination of quantum energy levels in atoms, molecules, semiconductors, etc. For example, in addition to their internal electronic motion, molecules possess vibrational and rotational degrees of freedom. Such motion is quantized, i.e., only motion corresponding to discrete rotational or vibrational energies is allowed. Spectroscopy, which excites transitions between these quantized states, is the primary tool in elucidating the energy-level spacing. These, in turn, are useful in determining bond strengths and overall molecular structure.

"Traditional" spectroscopy can be described as energy or frequency resolved because measurements associated with this type of spectroscopy involve spectrally narrow light that is tuned across discrete energy levels. These measurements can be carried out with pulsed light sources to provide

time-resolved kinetic information about processes that are statistical in nature. "Ultrafast" spectroscopy, on the other hand, involves temporally short (and therefore spectrally broad) light pulses, which are used to probe directly the dynamics of the system rather than the energy levels themselves. Rapid advances in laser technology over the past decade have resulted in the ability to produce pulses as short as 6 fs ($1 \text{ fs} = 10^{-15} \text{ s}$), and pulses of width 60 fs are now produced routinely in many laboratories around the world (see ULTRASHORT PULSE PHENOMENA).

The advantage of using ultrashort pulses is that they open the door to investigating the dynamics of the system directly, i.e., the movement of individual particles such as electrons or atoms. From the perspective of classical mechanics, a short pulse whose duration is on the same time scale as the motion of a particle in a confined system could be used to probe the dynamics of the particle directly. For typical atomic speeds of the

order of 10 000 m/s ($= 0.1 \text{ \AA}/\text{fs}$), laser pulses 10 fs in duration achieve 1- \AA spatial resolution, a range that is of great scientific interest in physics and chemistry. Ultrafast spectroscopic techniques have been used to observe rotational and vibrational dynamics in molecules. Electronic motion has been explored in semiconductor systems. The key is that the duration of the laser pulses must be shorter than the time scale of the dynamics that one wants to observe. Time scales of some physical and chemical processes are displayed in Fig. 1.

In summary, ultrafast laser spectroscopy has become a very useful tool in the study of the dynamics of atoms and molecules in a range of environments from gas phase to solid state. Results from these types of ultrafast studies have been loosely classified as femtochemistry, when chemical reactions are involved, and femtophysics, when the interaction between ultrashort laser pulses and matter is being studied.

The rest of the article is as follows. Section 1 covers the physical basis for ultrafast spectroscopy and contrasts it with frequency-resolved spectroscopy. In Sec. 2 the experimental setup required for ultrafast spectroscopy is described along with a discussion of the pump-probe technique. Results from an experiment on iodine are shown in Sec. 3, where both the vibrational and rotational dynamics are obtained. In Sec. 4 studies of various different chemical reactions in the gas phase are presented. Additional applications of ultrafast spectroscopy to condensed phases and biological systems are outlined in Sec. 5.

1. PHYSICAL FRAMEWORK AND EXAMPLES

Ultrafast spectroscopy is based on the use of light pulses that have very short temporal duration to interrogate matter. These pulses,

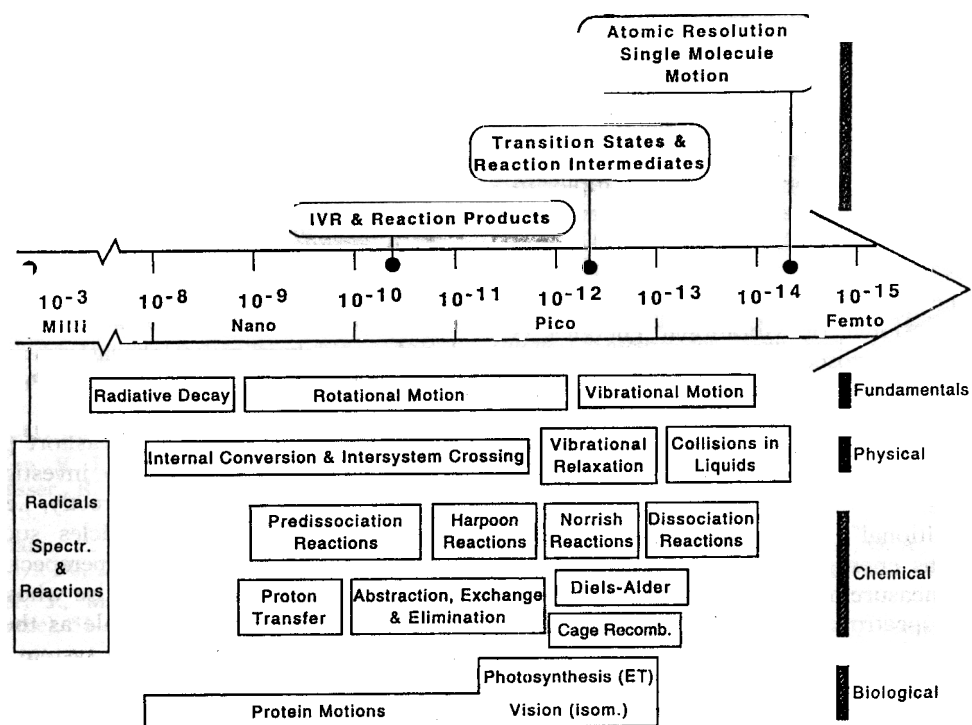


FIG. 1. Time scales and scope of ultrafast phenomena in physical, chemical, and biological changes. On the upper side of the arrow of time, we display the fundamental elements for the dynamics of the chemical bond, defining the scales for intramolecular vibrational relaxation (IVR), transition states, and single-molecule motion in femtochemistry. The time scales for the vibrational and rotational motions are shown. Below the arrow of time, examples of studies of physical, chemical, and biological motions are given (Zewail, 1996.)

being very fast compared to the underlying dynamics of the system, are capable of taking "snapshots" of the atomic motion. A collection of snapshots taken at subsequent times can be thought of as a "movie" of the dynamics as a function of time. Each snapshot implies a degree of localization of the system in space that must be consistent with Heisenberg's uncertainty principle. To illustrate the advantages of ultrafast spectroscopy and explore some of its implications, a quantum-mechanical formalism is required (for a review see QUANTUM MECHANICS).

Quantum mechanically speaking, the fact that short pulses probe dynamics and long pulses probe energy levels is indicative of the uncertainty principle, that time and energy resolution are related to each other through the Fourier transform. For example, a very short pulse (on the order of 10^{-15} s) possesses a broad energy bandwidth, which spans the whole visible spectrum. In contrast, a longer pulse (on the order of 10^{-9} s) possesses a much narrower spectrum. This relationship can be illustrated in a completely general manner by showing the effect of the laser-pulse width (time duration) on the transition probability from one state χ_0 of a system with energy E'_0 to other states $\varphi_0, \varphi_1, \varphi_2$, etc. with corresponding energies E_0, E_1, E_2 , etc. First-order perturbation theory can be used to describe the transition probability from the initial state χ_0 to each state in the upper potential induced by the laser pulse that is nearly resonant with the transition (i.e., the photon energy $\hbar\omega$ is roughly the same as the energy difference $E_n - E'_0$ between the energy levels). The laser pulse is assumed to be a Gaussian, $\mathcal{E}_0 \exp[-t^2/\alpha\tau^2] \times \cos(\omega t)$, with a temporal full width at half maximum (FWHM) τ . The resulting wave function after excitation can be written as a superposition of the eigenstates of the system:

$$\psi = \sum_{n=0} a_n \varphi_n, \quad (1)$$

where a_n are the coefficients (or amplitudes) of the eigenstates φ_n . These coefficients, whose moduli squared represent the populations or occupation probabilities of the individual eigenstates after the pulse is applied, can be determined from the following first-order perturbation-theory formula:

$$a_n = C \langle \varphi_n | \chi_0 \rangle \int_{-\infty}^{\infty} \exp[-i(E_n - E'_0)t/\hbar] \times \exp(-t^2/\alpha\tau^2) \cos(\omega t) dt, \quad (2)$$

where C is a constant including such factors as the field amplitude of the pulse and the electronic transition dipole moment, and α is a constant equal to $2\pi^2/\ln(2)$. The term $\langle \varphi_n | \chi_0 \rangle$ is called the "Franck-Condon" factor and is just the overlap integral between the initial and final states. Evaluating the integral in Eq. (2) gives

$$a_n = C \langle \varphi_n | \chi_0 \rangle \exp[-(\omega_n - \omega)^2 \alpha \tau^2 / 4], \quad (3)$$

where $\omega_n = (E_n - E'_0)/\hbar$ is defined as the Bohr frequency. Note that in evaluating the coefficients a_n all we have done is evaluate the Fourier transform of a Gaussian function (the importance of the Fourier transform and its relevance to the distinction between energy- and time-resolved spectroscopy is made clear below).

In the limit of an ultrashort pulse ($\tau \rightarrow 0$) the coefficients in Eq. (3) become

$$a_n = C \langle \varphi_n | \chi_0 \rangle. \quad (4)$$

Note that the newly created wave function can then be written from Eq. (1) as

$$\psi = C \sum_{n=0} \langle \varphi_n | \chi_0 \rangle \varphi_n. \quad (5)$$

Note also that the initial wave function can be expressed in terms of the excited eigenfunctions φ_n ,

$$\chi_0 = \sum_{n=0} \langle \varphi_n | \chi_0 \rangle \varphi_n. \quad (6)$$

Thus we see that a very short (delta function in time) pulse creates a wave packet ψ on the upper potential that possesses exactly the same shape as the initial wave function (to within an overall constant). Of course, this wave packet is not an eigenstate of the system but rather a *coherent superposition* of excited eigenstates. Over time, these states *dephase* with respect to one another, since the time dependence of the wave function is given by

$$\psi(t) = \sum_{n=0} a_n \exp(-iE_n t/\hbar) \varphi_n. \quad (7)$$

Such a wave function is called *nonstationary* since quantum-mechanical expectation values corresponding to physical observables such as position or momentum are not constant in time. This can be seen from the expression for the time dependence of an expectation value of some observable, say position R (i.e., the internuclear distance between the atoms in a diatomic molecule):

$$\langle \psi(t) | R | \psi(t) \rangle = \sum_{n=0} \langle \varphi_n | R | \varphi_n \rangle + 2 \sum_{m=1}^{m-1} \sum_{n=0} a_m^* a_n \times \cos[(E_m - E_n)t/\hbar] \langle \varphi_m | R | \varphi_n \rangle. \quad (8)$$

The first term on the right-hand side of Eq. (8) gives the average equilibrium distance of the motion and does not vary in time, but the second term does; this explicit dependence on time is responsible for the "wave-packet dynamics," in this case, the motion of the nuclei themselves. For example, in the case of a diatomic molecule whose nuclei move in a harmonic potential well, the movement of the wave packet is governed by the energy-level spacing ΔE ; the packet oscillates and returns to its original form after a time $\hbar/\Delta E$, assumed here to be 333 fs. Figure 2 shows the expectation value for the internuclear distance R as a function of time using Eq. (8). The dashed line shows the trajectory of a particle based on classical mechanics. Notice that when the motion is initiated by a short-time pulse ($\tau = 42$ fs), the motion is very similar to that of the classical particle; however, when τ is long (a time equivalent to two full periods of motion, here 667 fs), the expectation value is close to equilibrium and one is no longer able to measure the dynamics since essentially only a single eigenstate (a stationary state of the system) is excited.

In the limit of a very long pulse (frequency-resolved spectroscopy), i.e., $\tau \rightarrow \infty$, we get from Eq. (2)

$$a_n = C \langle \varphi_n | \chi_0 \rangle \delta(\omega_n - \omega), \quad (9)$$

where $\delta(\omega_n - \omega)$ is a delta function, which is always zero except when ω equals ω_n . Thus, unless the laser frequency exactly matches the difference in energy between states n and the ground state, there is no excitation. When the energy difference does match the

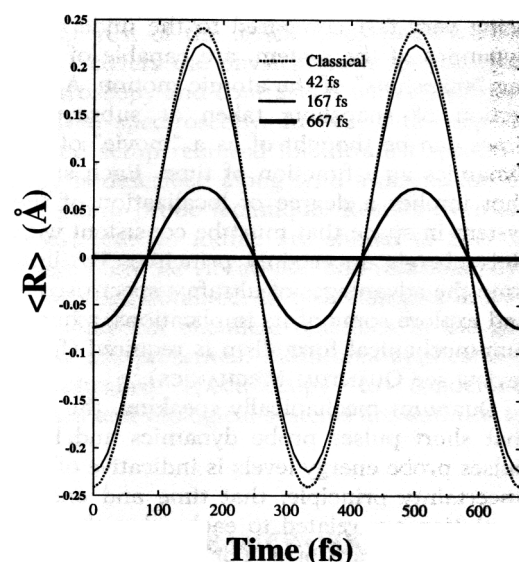


FIG. 2. Calculated expectation values for the average internuclear distance of a diatomic molecule when excited with pulses of increasingly longer temporal width [calculations based on Eq. (8)]. Notice that a 42-fs pulse generates a wave packet with dynamics that are very similar to those of a classical particle in the same harmonic potential. The data generated for the 667-fs pulse do not show the oscillatory motion because the wave packet formed is similar to an eigenstate of the potential.

laser photon energy $\hbar\omega$, only a single eigenstate is excited. This is a stationary state, and as such, the expectation values (momentum, position, etc.) do not change with time, unlike in a nonstationary state created from a short pulse (see, for instance, the 667-fs example in Fig. 2). For intermediate pulse lengths where τ is small enough that

$$\exp[-(\omega_n - \omega)^2 \alpha \tau^2 / 4] \gg 0 \quad (10)$$

for more than one level of energy E_n , a nonstationary state is created since more than one eigenstate will be appreciably populated.

Invoking the relationship between time and energy via the Fourier transform, it is easily shown that the longer the pulse, the more the wave packet in the upper state resembles a single stationary eigenstate rather than a coherent superposition. The shorter the pulse, the wider the frequency width, and the more the newly created wave packet in the upper state resembles the initial state of the system. Since the initial state of the

lower potential is not an eigenstate of the upper potential, but rather a superposition of eigenstates that resemble it, it exhibits dynamics.

1.1 Illustrative Example

A simple calculation based on the equations presented in the last section nicely illustrates this concept of time and energy resolution in spectroscopy. For illustration, consider the excitation of a diatomic molecule from its ground electronic and vibrational state to its first excited electronic state. The potential-energy curves associated with this system are depicted in Fig. 3. These curves are based on the Born–Oppenheimer approximation, which recognizes that nuclei in a molecule move much more slowly than

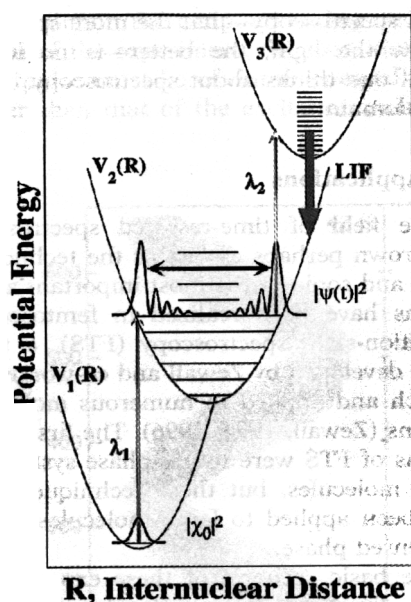


FIG. 3. Schematic of the potential-energy curves of a diatomic molecule with three distinct electronic states $V_1(R)$, $V_2(R)$, and $V_3(R)$. The electronic states provide a harmonic potential that keeps the nuclei bound and gives rise to vibrational energy levels. Ultrafast spectroscopic information from this system can be obtained by excitation at λ_1 from the ground electronic state into the intermediate potential $V_2(R)$. This excitation generates a wave packet that oscillates in time. Probing of the wave-packet motion is accomplished by a second pulse of wavelength λ_2 that populates the third electronic state. Signal from the third electronic state is measured as the intensity of the laser-induced fluorescence (LIF) from $V_3(R)$.

electrons; therefore, one can map the electronic potential energy as a function of internuclear distance. On these potential curves, the corresponding vibrational levels are drawn. The electronic states are shown as harmonic oscillators $V_1(R)$, $V_2(R)$, and $V_3(R)$, which resemble the potential energy that the nuclei experience in a molecule, neglecting anharmonic terms that are important at high vibrational energies (see MOLECULAR SPECTROSCOPY). Only the initial state χ_0 is assumed to be populated before the laser pulse excites the system; its wave function is also shown in Fig. 3. The first excited electronic state (with a different electronic configuration) is found at a higher energy and slightly larger equilibrium bond length. These differences are typical for molecules because a change in electronic configuration affects the interatomic interactions.

Photon absorption from the ground electronic state is assumed to proceed through a vertical transition to the upper state, invoking the Franck–Condon approximation. The implication here is that changes in electronic configuration take place much faster than nuclear motion, and therefore the nuclei are essentially “frozen” in place during the electronic transition. When the light source is monochromatic, only one vibrational state in the upper electronic potential can be excited. For ultrashort pulses, having a broad spectral bandwidth, more than one state may be populated at the same time as described by Eqs. (1) and (2). For the calculations presented here the energy displacement (i.e., the energy difference between the potential-well minima) is taken to be $15\,770\text{ cm}^{-1}$ (about 2 eV). The reduced mass and the quantum energy-level spacing of both potentials ($\omega = 1.9 \times 10^{13}\text{ Hz}$, equivalent to a 333-fs oscillation period) roughly correspond to those of the iodine molecule (I_2).

Figure 4 (left-hand side) shows (from top to bottom) the wave packet $|\psi(x)|^2$ created on $V_2(R)$ after application of 42-, 167-, and 667-fs FWHM Gaussian pulses ($\frac{1}{8}$, $\frac{1}{2}$, and 2 times the molecular oscillation period of I_2 , respectively). The shortest of these pulses creates a nearly perfect Gaussian wave packet on $V_2(R)$ as shown in the top left frame of Fig. 4; this wave packet is virtually identical to $|\chi_0|^2$, the ground state of $V_1(R)$, as expected from Eqs. (4)–(6). If the pulse is lengthened, the wave packet starts to look less like $|\chi_0|^2$

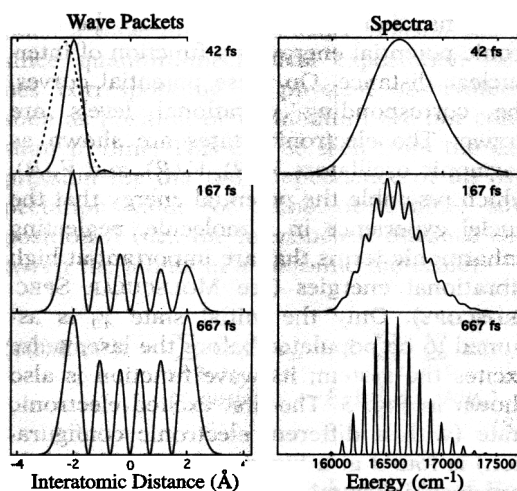


FIG. 4. (a) Calculation of wave packets pumped from the ground to excited electronic state by 42-, 167-, and 667-fs pulses [using Eqs. (1) and (3)]. The packet formed by the 42-fs pulse is very similar to the ground-state wave function $|\chi_0|^2$ shown with a dashed line. (b) Corresponding spectra for these same pulse lengths [using Eq. (11)].

and more like a single eigenstate on $V_2(R)$ [see Eq. (9)]. The laser-pulse frequency for this example was chosen to match the energy difference between the ground state of $V_1(R)$ and the 5th eigenstate φ_5 of $V_2(R)$. The wave function shown in Fig. 4 (bottom left) for the 667-fs pulse was produced by a sufficiently long pulse that the condition in Eq. (10) was satisfied for only one energy, E_5 ; therefore, the excited wave packet in this case is essentially identical to the eigenstate $|\varphi_5|^2$. Unlike the wave functions shown for the 42- and 167-fs pulses, which are linear superpositions of the $V_2(R)$ eigenstates, the wave function produced by the 667-fs pulse is essentially a stationary state and will not change with time.

Scanning the frequency of the excitation laser, one obtains an absorption spectrum of the system. The spectra depend on the temporal duration of the laser pulses because of the time-energy uncertainty. This dependence is included in the a_n terms [Eq. (3)]. The spectra can be calculated simply by the sum

$$A(\omega, \tau) = \sum_{n=0} |a_n|^2. \quad (11)$$

In Fig. 4 (right-hand side) spectra for the

three different laser-pulse widths are shown. The key point is that the shortest pulse (42 fs) provides the least spectral resolution, 353 cm⁻¹ FWHM. The longest pulse (667 fs) provides much sharper spectral lines, 22 cm⁻¹ FWHM, and each line corresponds to a particular $\chi_0 \rightarrow \varphi_n$ transition. Long-pulse excitation corresponds to a frequency-resolved spectrum; no dynamics can be observed because only single eigenstates are excited. In short-pulse excitation, where spectral resolution is very poor, the wave packet created on $V_2(R)$ does exhibit dynamics as the laser pulse excites a superposition of eigenstates.

It should be emphasized again that the spectrally broad pump pulse is responsible for the creation of the wave packet. A long pulse (in time) would excite only a single eigenstate on $V_2(R)$, and therefore no dynamics would be observed using the probe pulse. Thus the normal way of thinking in traditional spectroscopy—that the more spectrally narrow the light, the better—is no longer true if one thinks about spectroscopy in the time domain.

1.2 Applications

The field of time-resolved spectroscopy has grown perhaps as fast as the technology itself, and some of the most important applications have been realized in femtosecond transition-state spectroscopy (FTS), a technique developed by Zewail and co-workers at Caltech and applied to numerous molecular systems (Zewail, 1994, 1996). The first applications of FTS were to gas-phase systems of small molecules, but these techniques have now been applied to large molecules in the condensed phase.

The basic scenario of these experiments, which directly observe molecular dynamics, is as follows. A short (femtosecond) pump pulse excites the molecule from its (bound) ground electronic state to an excited state. As noted in the previous discussion of the laser pulse inducing a transition between two displaced harmonic oscillators, a wave packet is created “upstairs” by the pump pulse. The wave packet, being nonstationary, moves on the upper electronic state potential as a localized probability density.

The motion of the wave packet ($|\psi(x,t)|^2$) as a function of time in the upper potential

is illustrated in Fig. 5 where $\psi(x,t)$ is given by Eqs. (1) and (2). For this illustration, the initial wave packets were generated with 42-, 167-, and 667-fs pulses, as shown in Fig. 4. Notice that for the shortest pulse one obtains the best localization of the wave packet, and its motion is most similar with that of a classical particle (see Fig. 2). The intermediate (167-fs) pulse shows a more diffuse wave packet. However, long-pulse excitation leads to a wave packet that is essentially an eigenstate of the upper potential and is therefore stationary in time. Figure 5 demonstrates how ultrafast excitation results in the creation of a time-evolving wave packet. The periodicity of the motion is determined by the energy difference among the states composing the wave packet [see Eq. (8)]. Monitoring the subsequent motion of the system requires an additional ultrashort pulse that is fired at different delay times as described below.

To maintain the temporal and spatial resolution of the experiment, the monitoring or probe pulse must be of duration equal to or shorter than that of the excitation pulse. In

general, the second pulse, of wavelength λ_2 , induces a transition from the intermediate state $V_2(R)$, where the wave packet evolves, to a higher electronic state that is easily detected by fluorescence or ionization (see Fig. 3). When the initial wave packet is highly localized, as represented here with the 42-fs excitation, there are times when the wave packet is inside the probing region, marked by the dashed lines in Fig. 5, and other times when the wave packet is outside this region.

The signal one expects from these types of experiments can be simulated using second-order perturbation theory (see QUANTUM MECHANICS), which takes into account transitions $V_1(R) \rightarrow V_2(R)$ and $V_2(R) \rightarrow V_3(R)$ as a function of the delay between the pump and probe pulses. Results based on the wave-packet motion are shown in Fig. 6. The shorter the pump and probe pulses, the better the wave-packet localization and the better the modulation depth in the oscillatory dynamics. For long-pulse excitation, no dynamics is observed in the signal. Notice that the results of the pump-probe experiment

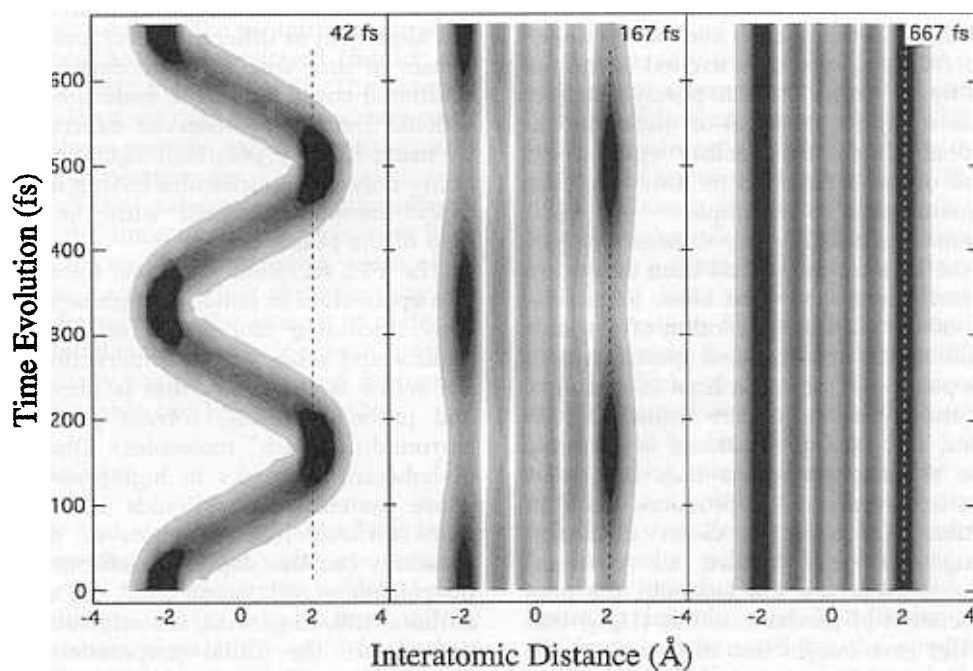


FIG. 5. Calculated wave-packet motion for excitation of three different pulse widths [using Eq. (7)]. Darker shades indicate higher probability densities. Notice that the 42-fs wave packet is very localized, while the 667-fs one is spread across the well and shows no signs of dynamics.

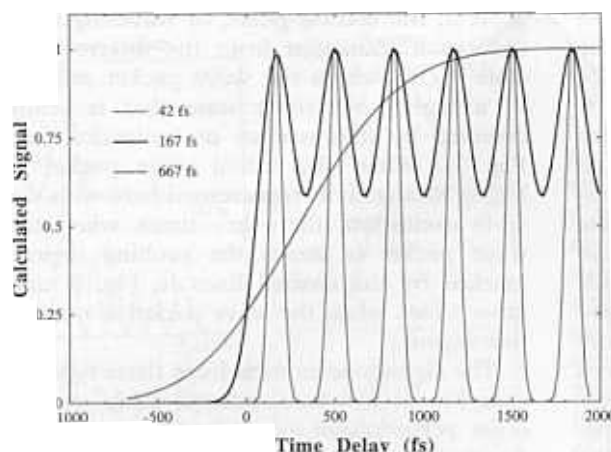


FIG. 6. Calculated pump-probe signal for three different pulse durations. In all cases the pump and probe lasers are assumed to have the same pulse width and intensity. Notice the changes in the rise times and the changes in modulation depth as the pulses increase in duration.

are analogous to a direct measurement of the interatomic spacing given by $\langle R \rangle$ in Eq. (8) and in Fig. 2.

Vibrational motion in the excited transients has been observed in many systems. The FTS pump-probe technique was used to observe vibrational motion in the excited B state of iodine (Dantus *et al.*, 1990) (see below), in predissociative systems such as sodium iodide (NaI) (Rose *et al.*, 1988), and in purely dissociative systems such as cyanogen iodide (ICN), where the excited state accessed by the pump pulse is purely repulsive (Dantus *et al.*, 1987). In all of these (one-dimensional) cases, the nuclear motion was mapped out as a function of time using the aforementioned FTS technique.

Beyond these simple one-dimensional systems, the FTS technique has been applied to more complex systems that allow for examination of the vibrational motion of a transition state. With time-resolved spectroscopy it is now possible to learn, at least in principle, about the dynamics of the transition-state complex, i.e., how these atoms are moving relative to one another as they are transformed from reactants to products. Such information may bring us closer to understanding the very nature of chemical reactions themselves. For example, the photodissociation of mercuric iodide (HgI_2) into I and HgI gave insight into the nature of the $[\text{I}-\text{Hg}-\text{I}]^{\ddagger}$ transition-state complex by again looking at the vibrational dynamics (Dantus *et al.*, 1989).

Molecular rotation has also been observed

with ultrafast pump-probe spectroscopy. However, this process is on a different time scale because rotational energy spacings transform into much longer times, on the order of 100 ps. The basic premise of rotational spectroscopy is that the pump pulse excites a coherent superposition of rotational states, a wave packet, which initially dephases (since molecules possessing different angular momenta rotate away from their initial alignment at different rates) and later rephases at time intervals that depend on the rotational constants of the molecule. The rotational motion is observed experimentally by using linearly polarized light pulses that excite only those molecules having transition dipole moments aligned with the electric field of the pulse.

The FTS technique has also found extensive application in condensed-phase spectroscopy, including elucidation of solvent dynamics and solute-solvent interactions (here the solute is the entity that is photoexcited and probed, and the solvent provides the surrounding "bath" molecules). Observation of coherent dynamics in high-pressure gas-phase systems or in liquids is inherently more difficult than in gases at moderate pressures because dephasing effects induced by collisions will "wash out" the coherent motion. Still, in general, for sufficiently short times after the initial preparation of the wave packet with the pump pulse, motion of the vibrational and rotational transients can be observed before complete relaxation takes place.

2. EXPERIMENTAL TECHNIQUES AND METHODS

The time scale for measurements using ultrafast spectroscopy is determined by the spacing between the energy levels of the system under study, as discussed in the Introduction. Typically, ultrafast spectroscopy measurements temporally resolve dynamics shorter than 10^{-12} s (1 ps). Given that most measurement equipment, such as oscilloscopes, have response times in the nanosecond time scale, special experimental arrangements are required in order to achieve femtosecond time resolution. In this section we describe how ultrafast laser pulses are generated and how they are used to measure molecular dynamics.

2.1 Ultrafast Laser Systems

There have been great advances recently in the generation of ultrafast laser pulses. This progress has been fueled to a large extent by the communication industry (primarily work by Shank, Ippen, and their colleagues at Bell Laboratories) with the goal of decreasing laser-pulse duration so that more information can be transmitted within a given time interval. The evolution of these laser systems has been reviewed (Squier and Mourou, 1992; Fleming, 1986; ULTRASHORT PULSES). Here we concentrate on the principles of these systems and the requirements of ultrafast spectroscopy.

One of the consequences or manifestations of the uncertainty principle is a limit imposed on the temporal pulse width of laser pulses such that their duration may not be any shorter than the inverse of their frequency bandwidth. For pulses with a Gaussian intensity profile in time and frequency, this relationship can be simplified to

$$\Delta\nu\tau \geq 2\ln(2)/\pi, \quad (12)$$

where $\Delta\nu$ and τ are the FWHM of the laser-pulse frequency and time width, respectively. The shortest pulse measured to date had a pulse duration of 5 fs (Baltuska *et al.*, 1997), and the record since 1987 was 6 fs (Fork *et al.*, 1987), corresponding to frequency bandwidths of 8.8×10^{13} Hz (2940 cm^{-1}) and 7.3×10^{13} Hz (2450 cm^{-1}), respectively, according to Eq. (12). The generation of such

short pulses presents great technical challenges (see ULTRASHORT PULSE PHENOMENA).

Femtosecond pulse generation is achieved in an oscillator cavity that has a very broad gain bandwidth and contains a nonlinear optical element whose properties are highly dependent on laser peak intensity. This arrangement favors the propagation of short pulses (high peak intensity) compared to continuous-output operation. There are many successful oscillator designs of this type; while some use laser dyes, others may be all solid state, even imbedded in optical fibers.

Femtosecond oscillators are capable of directly producing very short pulses (down to 8 fs), but energies are typically less than a nanojoule per pulse. Ultrafast spectroscopic measurements require high-energy pulses, and so the output of the oscillator needs to be amplified. The most successful technique for this uses grating pairs to lengthen the pulses temporally (Squier and Mourou, 1992). These "stretched" pulses are then amplified to millijoule levels and compressed back to the femtosecond time scale. By this method, millijoule pulses as short as 20 fs have been produced (Backus *et al.*, 1995).

Tunability of femtosecond laser systems may be achieved by continuum generation, whereby a very intense femtosecond pulse is focused on a transparent medium such as a quartz window and emerges as a white light pulse containing all wavelengths within the window of transmittance of quartz. The laser pulse induces a very rapid change in the refractive index of the medium, causing it to act as an ultrafast shutter. Because of the transform limit relationship between the time and energy bandwidths, this results in a large increase in the pulse bandwidth; conversion efficiency is very high, approaching 100%. Spectral selection from the continuum is achieved by filtering. If desired, more intense pulses can be generated by optical parametric amplification. In this process, a relatively weak (seed) pulse is mixed with a high-intensity pulse in a nonlinear optical medium, resulting in a pulse having a higher intensity than the seed. The fundamental of the laser can be used for the amplification pulse, and judicious selection of the frequency of the seed pulse will allow quite intense pulses to be produced at a given wavelength.

2.2 Detection in Ultrafast Spectroscopy; the Pump-Probe Method

In general, ultrafast spectroscopy has been associated with time scales shorter than picoseconds. This makes it useful for the study of molecular motion (see Fig. 1)—for example, rotation (picosecond) and vibration (femtosecond). The second major application is to electronic signals extending to the terahertz regime and beyond. These frequencies are considered ultrafast because one is no longer able to use conventional equipment for their measurement. The state of the art in photon detectors is still, as of 1997, lagging by almost three orders of magnitude behind the generation of short pulses. This fact has forced experimental groups to find techniques that depend on two or more ultrashort pulses to initiate and monitor a process; the time resolution in the resulting signal is then independent of the detection method. The most common of these arrangements is known as the pump-probe technique. This technique, in fact, has been critical in the advancement of time-resolved spectroscopy since 1949 when millisecond resolution was first achieved (Porter, 1950).

In the pump-probe method, the time resolution is determined by the convoluted temporal width of the pump and probe laser pulses, the degree of experimental control over the time delay between them, and their relative temporal jitter. Present systems for ultrafast spectroscopy have been able to produce pulses as short as 5–6 fs, with jitter and time-delay control better than a single femtosecond (Baltuska *et al.*, 1997; Fork *et al.*, 1987). This outstanding level of control is achieved by the use of arrangements such as the Mach-Zehnder interferometer shown in Fig. 7. An intense femtosecond laser pulse emerging from the amplifier is split by a partially reflective optic into two pulses that follow different paths in the interferometer. While in the interferometer, techniques based on nonlinear optics are used to change the wavelength of the laser pulses (if required by the particular experiment) while maintaining their pulse duration and timing of each relative to the sibling pulse. The pulses are later recombined using a second partially reflective optic before being steered to the sample region. The time delay between the pump and probe lasers is deter-

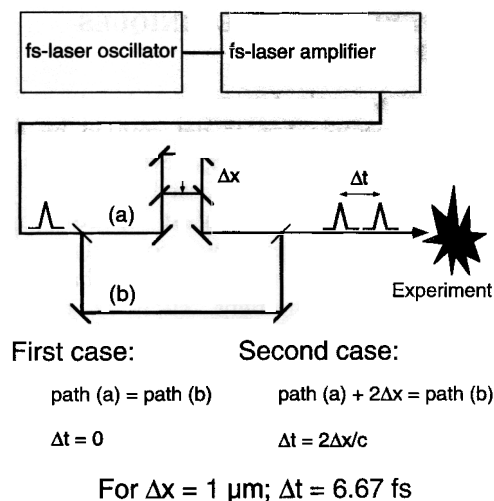


FIG. 7. Pump-probe experimental setup showing a typical Mach-Zehnder interferometric arrangement used to control the timing between pump (path a) and probe (path b) laser pulses.

mined by the position of a computer-controlled optical-delay line located in one of the arms of the interferometer. The principle of the time delay is that the speed of light is constant and that spatial displacements correspond directly to temporal delays. For a typical step of $1 \mu\text{m}$, a pulse is delayed by 3.3 fs. Because the light traverses the optical delay line twice, the corresponding delay is 6.67 fs (see Fig. 7).

Notice that the time resolution of pump-probe experiments depends on the time delay between the pump and probe pulses and not on the temporal response time of a detector. In fact, these experiments are independent of the response time of photon detectors or signal-processing electronics. This has allowed pump-probe experiments to be carried out in conjunction with a number of other spectroscopic techniques, e.g., absorption, emission, laser-induced fluorescence, ionization, and Raman spectroscopy.

3. ULTRAFAST SPECTROSCOPY OF MOLECULES

Ultrafast molecular spectroscopy is the time-domain analog of frequency-resolved spectroscopy (see MOLECULAR SPECTROSCOPY). Electronic, vibrational, and rotational

transitions are interrogated, but in ultrafast spectroscopy, coherence among the quantum states leads to time-dependent dynamics that can be directly associated with the classical mechanical motion. Among the advantages of time-domain spectroscopy is the complete separation of vibrational and rotational information, which may be obscured in frequency-resolved spectroscopy of molecules at room temperature. This effect is illustrated for the diatomic iodine molecule, where it is shown that one can measure rotational spacings of 0.027 cm^{-1} with laser bandwidths four orders of magnitude larger.

3.1 Ultrafast Rotational Spectroscopy

The electronic excitation of gas-phase iodine molecules from the ground state to the B state occurs in the 500–630-nm wavelength region. Rovibrational spectroscopic lines with a typical density of 100 lines per inverse centimeter can be resolved by excitation with narrow-bandwidth light. Even though the molecule is a simple diatomic, the interpretation and assignment of these spectral lines is not straightforward because of the hundreds of rotational levels associated with each vibrational level. When the molecule is excited with an ultrafast laser pulse, the bandwidth is orders of magnitude broader than the spacing between spectroscopic lines, which are therefore not observed (see Fig. 4 for example). However, ultrafast pulse excitation results in a coherent superposition of rotational and vibrational quantum states. Probing of this coherence in the temporal regime can be used to obtain the energy-domain information with the same accuracy as the frequency-resolved methods.

In Fig. 8, the relevant electronic states of iodine are presented; the arrow corresponds to excitation of the ground-state iodine molecule to the excited B state. The vibrational spacing in the B state of iodine at 620 nm is 110 cm^{-1} ; the spacing between rotational lines is $\approx 0.027 \text{ cm}^{-1}$. To observe ultrafast rotational spectroscopy, the laser pulses must be shorter than the inverse of the energy spacing between rotational lines, $(2B)^{-1}$ where B is the molecule's rotational constant, so that a coherence between rotational states may be achieved (Felker, 1992; Felker and Zewail, 1987). For diatomic iodine in the B state, this time corresponds to ≈ 270

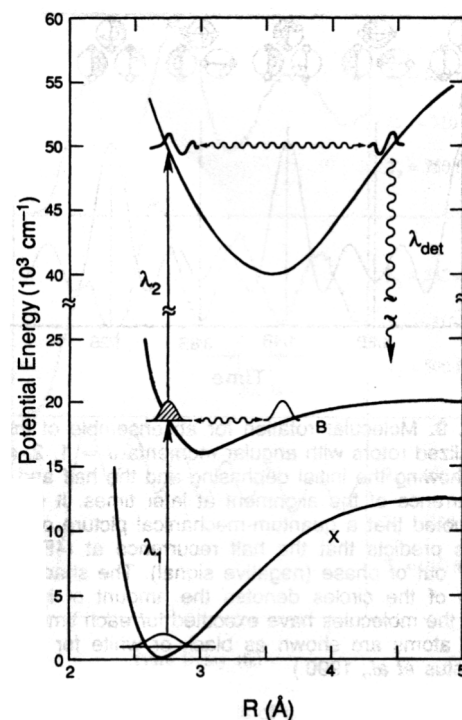


FIG. 8. Energy-level diagram for ultrafast spectroscopy of molecular iodine. The first femtosecond laser pulse (λ_1) excites the iodine molecules to the B $^3\Pi_{0+u}$ state, with accompanying vibrational and rotational excitation. The probing is carried out by a second femtosecond laser pulse (λ_2) that takes the wave packet to the upper fluorescent state. The signal detected (λ_{det}) is fluorescence from the upper electronic state. Absorption or ionization at λ_2 can also be used. (Dantus *et al.*, 1990.)

ps. For these experiments, a linearly polarized laser pulse excites only molecules that have their transition dipole moment μ parallel or nearly parallel to the polarization plane of the electric field of the laser pulse, \mathcal{E} , because the transition amplitude is determined by $\mu \cdot \mathcal{E}$. Initial excitation therefore selects an ensemble of aligned molecules. A second laser pulse, the probe, is then used to interrogate only previously excited molecules; because the probe pulse is also polarized, it is sensitive to the initial alignment. As the rotation of the ensemble evolves in time, the coherence decays because molecules having different degrees of rotational excitation will rotate at different rates.

Because all rotational levels are related to the same rotational constant by a factor of an integer quantum number J (the angular

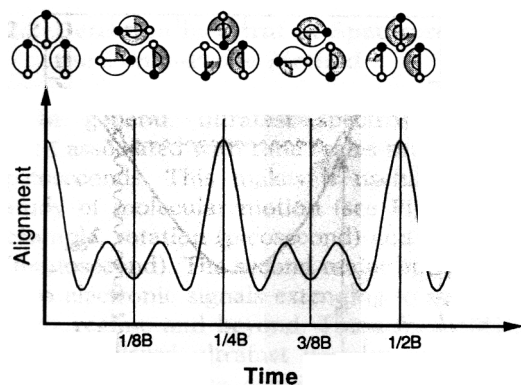


FIG. 9. Molecular rotation for an ensemble of three idealized rotors with angular momenta $J = 1, 2,$ and $3,$ showing the initial dephasing and the half and full recurrence of the alignment at later times. It should be noted that a quantum-mechanical picture of rotations predicts that the half recurrence at $(4B)^{-1}$ is 180° out of phase (negative signal). The shaded region of the circles denotes the amount of rotation that the molecules have executed for each time step. The atoms are shown as black or white for clarity. (Dantus *et al.*, 1990.)

momentum), the original alignment rephases after a time $(2B)^{-1}$ determined by the rotational energy constant $B.$ Figure 9 illustrates the principle of ultrafast rotational spectroscopy of a diatomic. For this illustration only

three molecules are depicted, with angular momenta $J = 1, 2,$ and $3.$ The molecules are assumed to be aligned at time $t = 0$ and free to rotate for all later times. After a time $(2B)^{-1}$ all molecules have executed an integer number of rotations that equals $J,$ thereby regaining the original molecular alignment. In an experiment, the initial alignment is achieved by the absorption of the linearly polarized pump laser. The probe laser is also linearly polarized and achieves a larger signal when it encounters molecular alignment (provided its polarization matches the orientation of the transition dipole). Notice that at times $(4B)^{-1}$ and $(2B)^{-1},$ the dipole moments are aligned and the signal achieves a maxima. The observation of rotational motion in real time is equivalently manifested in rotational spectroscopy where the spacing between rotational lines in the spectrum is $2B.$

In Fig. 10, experimental results obtained for iodine using 60-fs pulses are shown and compared to theoretical simulations (Dantus *et al.*, 1990). The results obtained when the pump and probe pulses are polarized parallel to each other, $I_{\parallel},$ are compared to those of perpendicular pump-probe polarization, $I_{\perp}.$ It can be seen that the rotational signatures are out of phase for these two cases. At early

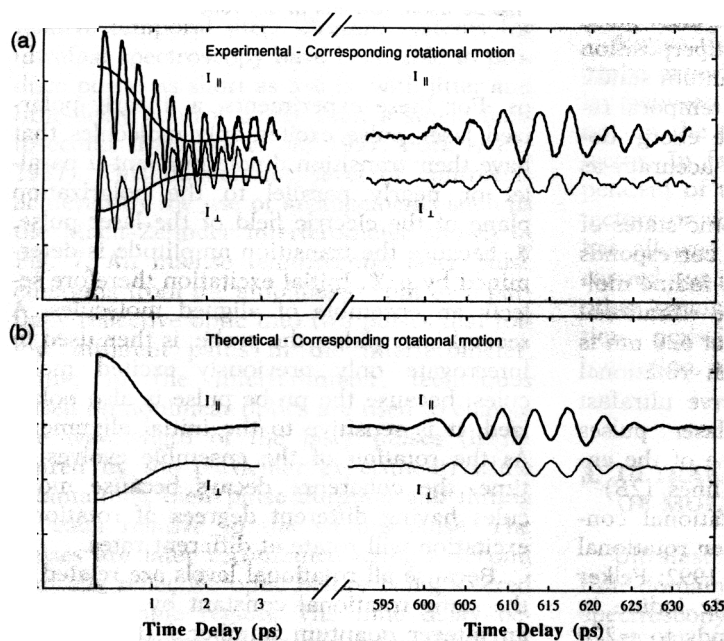


FIG. 10. Ultrafast study of molecular iodine with polarized lasers. (a) Transients showing the initial dephasing due to molecular rotation (left) and the appearance of full recurrences at a later time (right). Parallel (I_{\parallel}) and perpendicular (I_{\perp}) probe orientations are shown and are 180° out of phase, as expected. The rapid oscillations are due to vibrational excitation; six levels are reached (the solid line through these on the left is a guide to the eye). Half recurrences were observed experimentally but are not shown here. Note that the time scale is discontinuous. (b) Calculated results for rotational dephasing (left) and rephasing (right) assuming excitation of vibrational levels 7 to 12 and taking into account vibrational and rotational coupling and centrifugal distortion. (Dantus *et al.*, 1990.)

times, there is a clear dephasing of the original alignment. At long times, there is a series of alignments corresponding to $(2B_v)^{-1}$, where B_v is the corresponding rotational constant of the v vibrational level. Analysis of these data accounting for centrifugal distortion reveals the presence of vibrational levels $v = 7-12$.

Ultrafast rotational coherence has been used by various groups to study the structure of large molecules (more than 25 atoms) (Felker, 1992). The principle behind these measurements is the same as described here except for the contribution, in polyatomic molecules, of the other two rotational constants A and C . Because of the high degree of accuracy obtained and the complete isolation of rotational features, these experiments have been particularly useful in the determination of structures of weakly bound complexes such as those formed between amino acids that are hydrogen bonded with water molecules.

3.2 Ultrafast Vibrational Spectroscopy

When femtosecond pulses excite several vibrational levels, one is able to observe the molecular vibration of the wave packet. In Fig. 11, data are shown for excitation at different wavelengths (Bowman *et al.*, 1989). Notice that excitation with shorter wavelengths forms products having longer vibrational periods. This is due to the anharmonicity of the bound state. As the vibrational energy spacing decreases, the oscillation time increases. This is a characteristic of time-resolved spectroscopy and means that the resolution of the technique improves as the resolution of conventional (frequency-resolved) spectroscopy deteriorates (and vice versa).

Data such as those presented in Fig. 11 may be analyzed to obtain the shape of the electronic state. To invert the time-resolved data into the energy/frequency domain, one can simply take the Fourier transform of the data. In Fig. 12, experimental and theoretical plots are shown of data obtained for iodine molecules, having the pump and probe laser polarizations at the magic angle (54.7°) in order to cancel rotational contributions to the signal. Notice that the data show rapid oscillations modulated by a much slower oscillatory envelope. The high-frequency com-

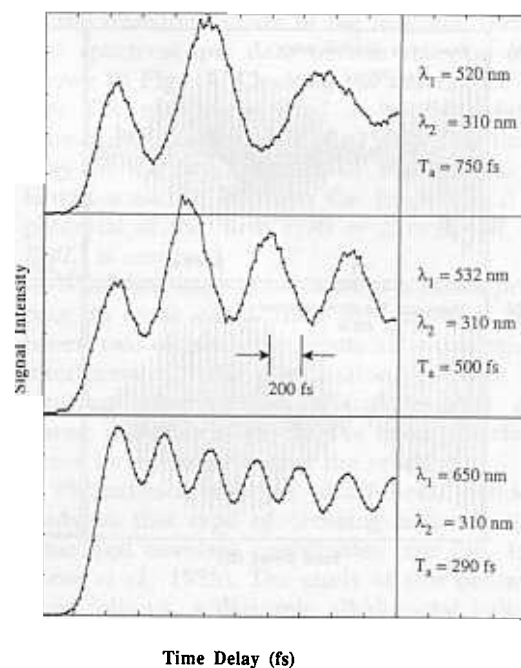


FIG. 11. Ultrafast transients of I_2 obtained at different pump laser wavelengths (λ_1). The time scale for the three traces is the same (200 fs/division). The periods are measured peak to peak between the second and third oscillations in order to avoid convolution effects. Complete analysis of these transients will give better values. (Bowman *et al.*, 1989.)

ponent corresponds to the average time of vibrations, while the long-time-scale modulation corresponds to the anharmonicity of the electronic state. In this case, one is able to determine that two vibrational states primarily contributed to these data and that the energy spacing between them correspond to the vibrational energy spacing of the molecule.

Comparing the Fourier-transformed data from ultrafast spectroscopy with that of high-resolution spectroscopy, one can observe the great simplification because of the separation of rotational and vibrational components. Rotational coherence occurs on a much longer time scale and can be discriminated against by setting the polarization vectors of pump and probe lasers at the magic angle.

In general, for large and heavy molecules where spectroscopic transitions overlap, ultrafast spectroscopy is clearly advantageous, allowing a complete separation between vi-

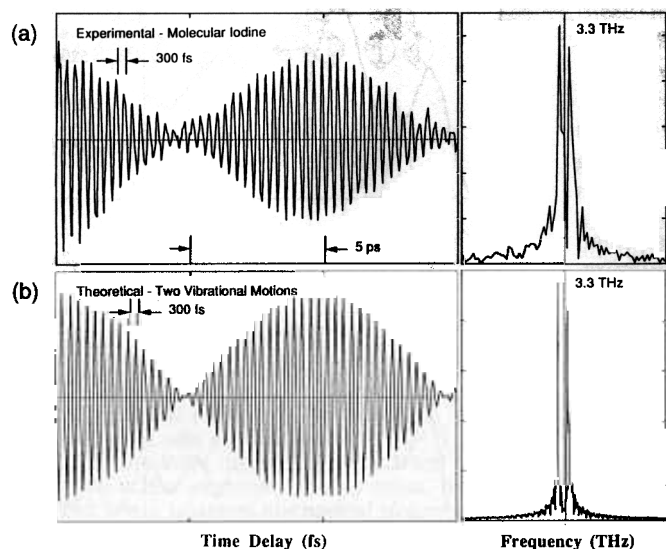


FIG. 12. (a) Ultrafast transients showing real-time vibrations of molecular iodine (left). The vertical scale represents the LIF amplitude, which is a probe of the internuclear distance. The corresponding Fourier transform is shown on the right. (b) Calculated results for excitation of a wave packet comprising the two principal vibrational frequencies and the corresponding Fourier transform. (Dantus *et al.*, 1990.)

brational and rotational information because of their differences in time scales.

3.3 Coherence and Dephasing

The ultrafast data presented in the previous section retain coherent excitation for a long time. This condition is easy to achieve in the gas phase at low pressures. When these types of experiments are carried out in high pressures approaching the density of the liquid phase, the coherence is lost by collisions. Experiments have been carried out to explore this transition from gas to liquid in

order to understand the behavior of molecules in solution (Zewail *et al.*, 1992; Lienau *et al.*, 1993; Lienau and Zewail, 1994, 1996; Materny *et al.*, 1996; Liu *et al.*, 1996).

As an illustration, Fig. 13 shows a study of the vibrational coherence of I_2 in the presence of argon gas at various pressures. At pressures below 10 bar, there is no collisional effect on the vibrational coherence because the average time between collisions is much longer than the time range probed in this experiment. However, an increase in pressure to 100 bar causes a loss of vibrational coherence as well as electronic quenching. Studies at higher pressures (not

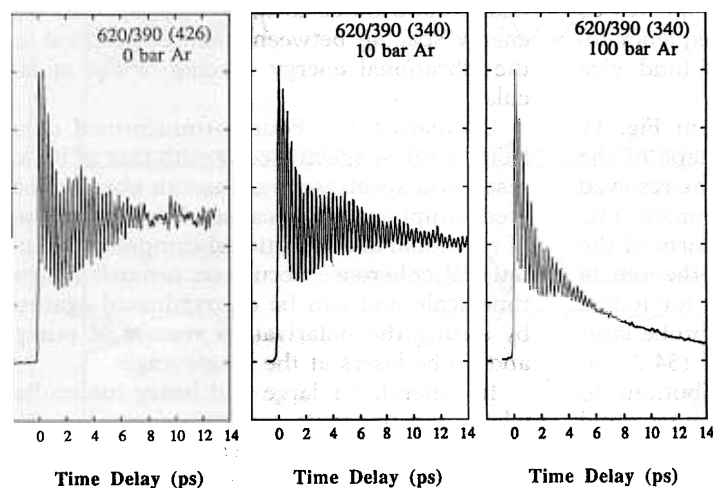


FIG. 13. Femtosecond transients of I_2 dissociation obtained as a function of increasing argon gas pressure. At high pressures the decay of the wave packet is evident. (Zewail *et al.*, 1992.)

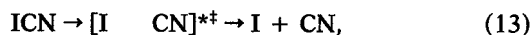
shown) have reproduced the dynamics observed in the liquid phase, where vibrational coherence survives for a few picoseconds (Zewail *et al.*, 1992; Lienau and Zewail, 1994, 1996; Materny *et al.*, 1996; Liu *et al.*, 1996).

4. CHEMICAL REACTIONS

One of the most important applications of ultrafast spectroscopy has been to the study of short-lived species such as transition states in chemical reactions. This type of experiment has allowed experimentalists to measure for the first time how long it takes to break or form a chemical bond. Ultrafast spectroscopy of chemical reactions, or femtochemistry, has allowed the study of many types of chemical reactions in real time, revealing details about the mechanisms involved (Manz and Wöste, 1995). There have been numerous studies from various research groups around the world, but the discussion here is limited to a few model cases without attempting a thorough review (see Further Reading).

4.1 Unimolecular Photodissociation along a Single Reaction Coordinate

One of the simplest chemical reactions is unimolecular photodissociation. The frequency-resolved spectrum associated with excitation to a repulsive electronic state leading to photodissociation is usually a featureless continuum that gives very little information about the dynamics involved. Ultrafast spectroscopy of the same system allows one to observe the progress of bond breakage, giving the researchers additional information about the electronic state such as the potential energy as a function of interatomic distance. In addition, the length of time required to break a chemical bond can be determined by this method. The first such study was carried out on the elementary reaction



where the $[\text{I} \cdots \text{CN}]^{\ddagger}$ species represent excited cyanogen iodide molecules (ICN*) in the process of becoming products. These transient species are sometimes referred to

as the transition states of the reaction. Ultrafast spectroscopic data of this reaction are shown in Fig. 14. Clocking the emergence of free CN radicals yielded a bond-breaking time of 205 fs (Rosker *et al.*, 1988). This time may be directly related to the repulsion length scale (L) between the fragments if a potential of the form $V(R) = E \exp[-(R - R_i)/L]$ is assumed.

Bond breakage is not always a direct process; in some cases, there are crossings between two or more electronic states, causing interference in the dissociation. The use of ultrafast spectroscopic techniques has allowed researchers to observe these interferences in real time during the reaction.

Photodissociation of alkali-metal halides leads to this type of crossing between the ionic and covalent coordinates (see Fig. 15) (Rose *et al.*, 1988). The study of this process is as follows. A diatomic alkali-metal halide (for example, NaI) is excited by a femtosecond pump laser to the covalent state, forming the activated complex $[\text{NaI}]^{\ddagger}$. Because of the crossing with the ionic state, the activated complex resides in the well; coherent excitation of the complex results in vibrations detectable by ultrafast pump-probe spectroscopy (see Fig. 15). The curve crossing allows a percentage of the vibrating molecules to escape from the well, producing $\text{Na} + \text{I}$. When the complex inside the well is probed, an exponentially decaying amplitude of coherent vibrations are observed. However, when one monitors the free sodium atoms resulting from the reaction, the signal increases in steps, reaching a plateau when all of the complex has escaped the bound well.

4.2 Unimolecular Photodissociation along Multiple Reaction Coordinates

When more than one reaction coordinate is available, the potential-energy surface of the reaction has a saddle point where progress along one of the coordinates is determined. The first direct spectroscopic probing of a saddle point was achieved in the photodissociation of HgI_2 , shown in Fig. 16 (Dantus *et al.*, 1989).

Time-resolved data from the reaction show vibrational motion in the nascent HgI fragment (300-fs period) as well as rotational motion (1.3-ps) caused by the torque of the

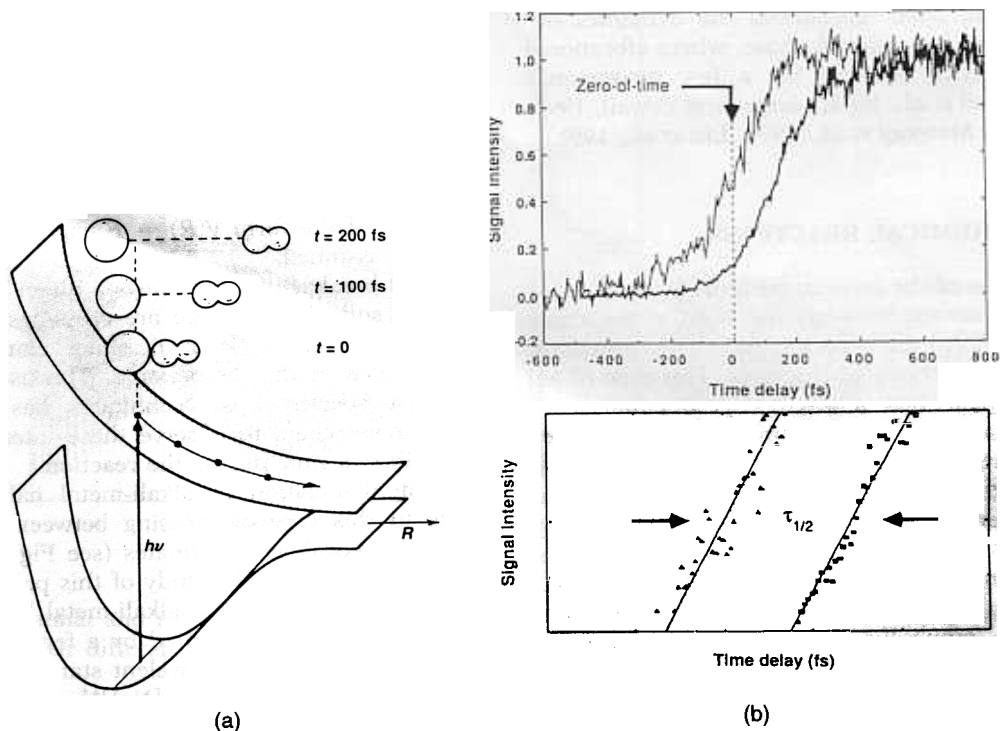


FIG. 14. Measurement of bond dissociation in the reaction $\text{ICN} + h\nu \rightarrow \text{I} + \text{CN}$. (a) A cartoon illustrating the experiment. A simple (slice through a) one-dimensional picture, with no angular dependence, is considered for the sake of clarity. At time $t = 0$ the laser pulse promotes the molecule to the upper potential energy surface. For $0 < t < \tau_{1/2}$, the bond stretches. By $t = \tau_{1/2}$, the bond is essentially broken. (b) Typical experimental results. The heavy line is the measured ICN transient, and the thin line is the reference $t = 0$ transient. The figure at the bottom shows a magnified view near $t = 0$. The observed delay for transform-limited pulses is 205 ± 30 fs. The error here is estimated from the scatter observed in several measurements. (Rosker *et al.*, 1988.)

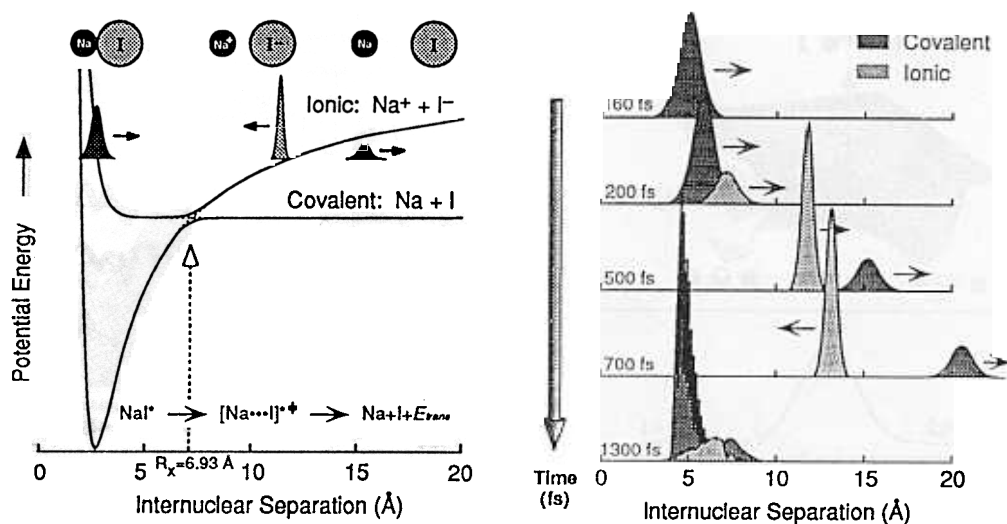
reaction. The large-amplitude rotational motion indicates that the activated complex has a bent geometry (see Fig. 16). The coherent vibrational motion in the product (all HgI fragments vibrating in concert) was unexpected and is the result of a prompt dissociation, which imparts an impulse perpendicular to the reaction coordinate. Coherence in the vibrational motion of products of reactions initiated with ultrafast lasers has now been observed in more complex systems including proteins such as rhodopsin (Wang *et al.*, 1994) and myoglobin (Zhu *et al.*, 1994).

4.3 Other Unimolecular Reactions

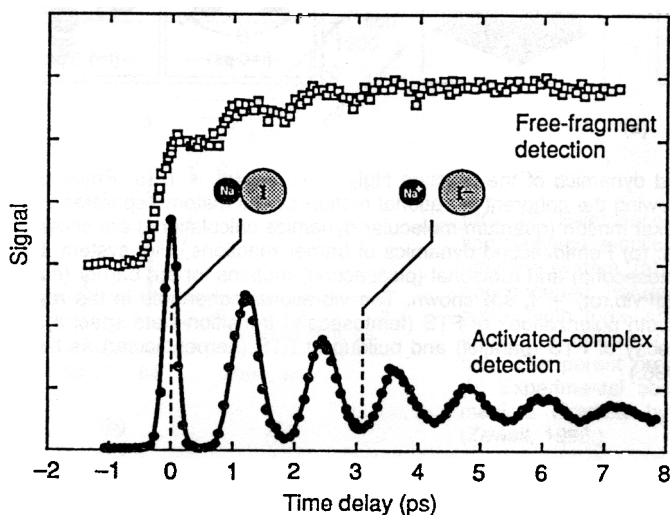
Ultrafast spectroscopic techniques have been used to study a wide variety of chemical processes such as isomerization, charge transfer, and proton transfer. Time resolu-

tion allows a direct assessment of the mechanism and dynamics of these reactions. This is particularly important in more complex reactions where one wants to determine the timing between multiple bond-breaking and bond-forming steps. Among these types of studies, the reaction of the cyclic carbonyl compounds is a classic example of mechanism determination (see Fig. 17) (Pedersen *et al.*, 1994).

Concerted chemical reactions, whereby more than one chemical bond is broken or formed in concert, are best studied by ultrafast spectroscopy in order to follow mechanisms and learn about the dynamics of such processes. One such reaction has been studied in which two bonds are broken and one is formed within a time that is much faster than molecular vibrations (< 60 fs). The photodissociation of methylene iodide,

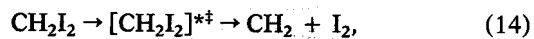


(a)



(b)

FIG. 15. Femtosecond dynamics of the reaction $\text{NaI} + h\nu \rightarrow \text{Na} + \text{I}$. (a) Potential-energy curves (left) and the “exact” quantum calculations (right) showing the wave packet as it changes in time and space. The corresponding changes in bond character are also noted: covalent (at 160 fs), covalent/ionic (at 500 fs), ionic (at 700 fs), and back to covalent (at 1.3 ps). (b) Experimental observations of wave-packet motion, made by detection of the activated complexes $[\text{NaI}]^{*\ddagger}$ or the free Na atoms. (Zewail, 1996.)



undergoes such a concerted mechanism. Upon 12-eV excitation by the pump pulse, iodine molecules are produced. Probing of these molecules reveals that all iodine mole-

cules are vibrating in concert (see Fig. 18) (Marvet and Dantus, 1996). The mechanism involves the concerted breaking of the two carbon-iodine bonds as the iodine atoms come into close proximity and form a bond. The fact that these steps occur simulta-

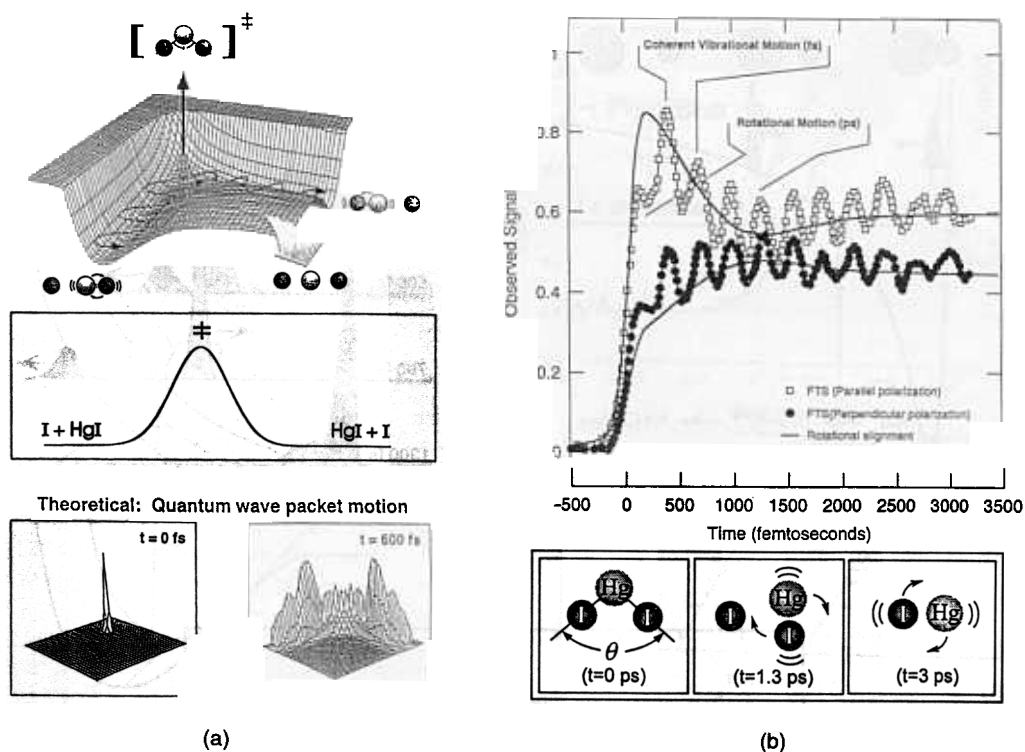


FIG. 16. Femtosecond dynamics of the reaction $HgI_2 + h\nu \rightarrow HgI + I$. (a) Potential energy surfaces, with a classical trajectory showing the coherent vibrational motion as the diatom separates from the I atom. Two snapshots of the wave-packet motion (quantum-molecular dynamics calculations) are shown for the same reaction at $t = 0$ and $t = 600$ fs. (b) Femtosecond dynamics of barrier reactions, $IHgI$ system. Experimental observations of the vibrational (femtosecond) and rotational (picosecond) motions for the barrier (saddle-point transition state) descent, $[IHgI]^{*‡} \rightarrow HgI(vib,rot) + I$, are shown. The vibrational coherence in the reaction trajectories (oscillations) is observed in both polarizations of FTS (femtosecond transition-state spectra). The rotational orientation can be seen in the decay of FTS (parallel) and buildup of FTS (perpendicular) as the HgI rotates during bond breakage. (Zewail, 1996.)

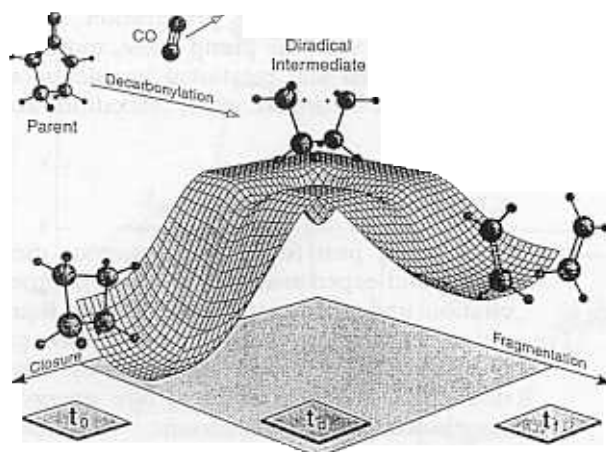
neously leads to a synchronized, or “coherent,” vibrational motion of the iodine molecules.

4.4 Bimolecular Reactions

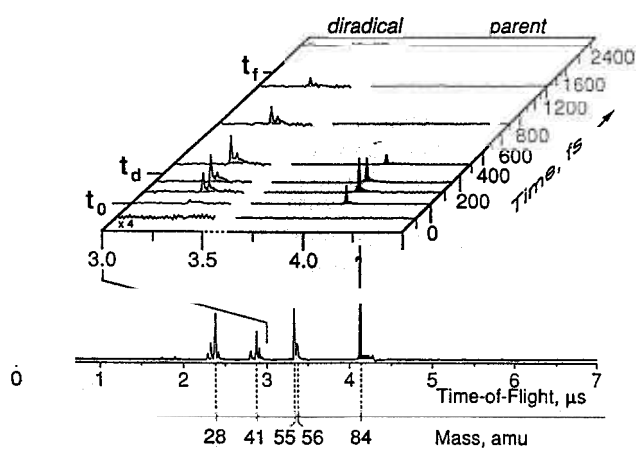
The study of bimolecular reactions using ultrafast techniques has been limited because of the difficulty of initiating these reactions with a laser pulse; they depend on collisions that occur at random times. This difficulty has been addressed by two separate approaches. One of them has been to take advantage of van der Waals complexes as precursors to the reaction (Hoffman *et al.*, 1990; Wittig and Zewail, 1996). If, for example, one wants to study the reaction between H and CO_2 , one can start with a precursor such

as $CO_2 \cdots HI$, which upon laser excitation releases the hydrogen reactant with a known kinetic energy. This technique helps establish the initial geometry, the energetics of the encounter, and the time of initiation of the bimolecular encounter. Figure 19 shows data from this type of study for the $CO_2 \cdots HI$ system. The emergence of the OH product, probed in this experiment by laser-induced fluorescence, is seen to occur within a picosecond of the initiation of the reaction.

An alternative approach for the study of bimolecular reactions in real time is to capture the collision pairs with an ultrafast laser pulse that excites the reactants to a new electronic state. This process is called photoassociation and has been shown to be useful in frequency-resolved spectroscopy to study molecules having dissociative ground



(a)



(b)

FIG. 17. Femtosecond dynamics of addition/cleavage reaction of the cyclobutane-ethylene system. (a) The PES showing the nonconcerted nature of the reaction, together with three snapshots of the structures at t_0 (initial), t_d (diradical), and t_f (final). The parent precursor is also shown. (b) Experimental observation of the intermediate diradical by mass spectrometry. (Zewail, 1996.)

states. It has also been demonstrated with ultrafast lasers (Marvet and Dantus, 1995), and the products show signs of coherence similar to those described earlier for bound molecular systems even though the initial state is a thermal distribution of incoherent states. In particular, a bulb containing gaseous mercury atoms has been shown to produce Hg_2 molecules in the state labeled V_1 in Fig. 20 under femtosecond laser excitation. Probing of these newly formed molecules is achieved by population depletion that causes a decrease in the laser-induced fluorescence (LIF) signal. The product molecules display rotational alignment that is similar to that

seen in rotational coherence spectroscopy; see Fig. 20.

5. OTHER APPLICATIONS OF ULTRAFAST SPECTROSCOPY

Ultrafast spectroscopy has also been used in the study of fast dynamics in liquids, clusters, semiconductors, and large biochemical systems. Observation of coherent dynamics in the condensed phase is inherently more difficult since dephasing effects induced by surrounding atoms and molecules will "wash out" the coherent motion. Still, for short

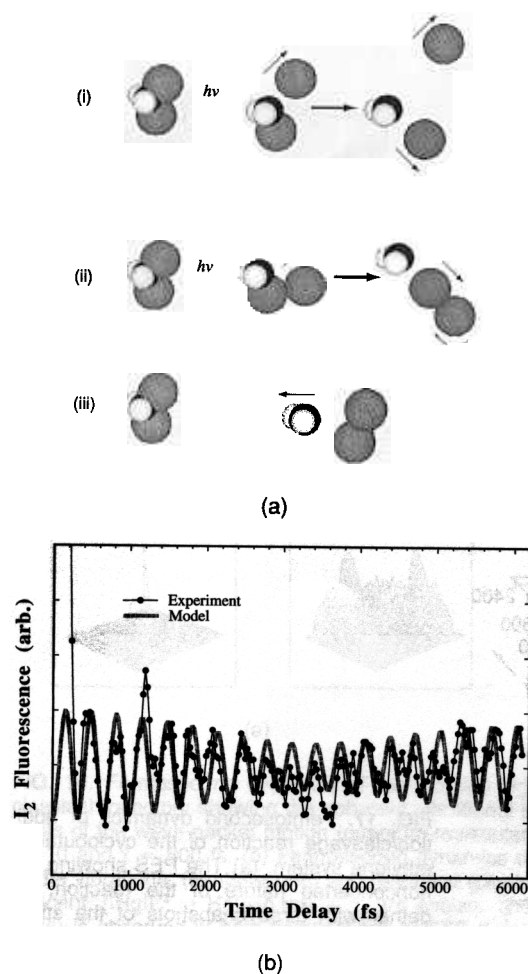


FIG. 18. Femtosecond dynamics of a concerted chemical reaction, $\text{CH}_2\text{I}_2 + h\nu \rightarrow \text{CH}_2 + \text{I}_2$. (a) Schematic of the reaction mechanisms. All fragments are drawn relative to carbene-fixed coordinates. (i) Stepwise (sequential) dissociation; the first iodine atom released has time to move away from the molecular fragment before the second carbon-iodine bond breaks. Molecular iodine is formed later by three-body collisions. (ii) Mechanism in which the first carbon-iodine bond is formed while the second iodine is still part of the molecule thus forming an ylide. This stage is concerted; subsequent breaking of the second carbon-iodine bond completes the reaction. (iii) Concerted bond breaking and formation process; breaking of the two carbon-iodine bonds is simultaneous with formation of an iodine-iodine bond. This mechanism would be expected to produce a molecular iodine product with a large degree of vibrational coherence. (b) Experimental measurement showing the prompt appearance of oscillatory dynamics due to the product I_2 molecules vibrating synchronously. The line is a model of the vibrational motion and the phase of these oscillations and is consistent with mechanism iii. (Marvet and Dantus, 1996.)

times after the initial preparation of the wave packet with the pump pulse, motion of the vibrational and rotational transients can be observed before complete relaxation takes place.

5.1 Liquids

Over the past few years numerous theoretical and experimental studies on photoexcitation and photodissociation in the liquid phase have been performed. In the gas phase, accurate measurements of the reactant and product in terms of how energy is distributed among electronic, vibrational, and rotational degrees of freedom is, at least in principle, possible. However, in liquids, where the solvent continuously interacts with the solute molecule in question, such detailed information is impossible. Nevertheless, ultrafast spectroscopy has been successfully used to learn about dynamical and energy-transfer processes between the solute and solvent and within the solute molecules themselves (Sitzmann and Eisenthal, 1989; de Boeij *et al.*, 1995).

Wave-packet motion has been experimentally observed in large dye molecules as well (Rosker *et al.*, 1986; Chesnoy and Mokhtari, 1988; Walmsley and Tang, 1990; Bigot *et al.*, 1991; Hashe *et al.*, 1995). Also, ultrafast pump-probe techniques have been used to study the time scales of solvation and vibrational relaxation of photoexcited dye molecules in liquids (Bingemann and Ernstring, 1995). Femtosecond studies of chemical reactions in liquids include the photodissociation of $\text{I}_3^- \rightarrow \text{I}_2^- + \text{I}$; here, the transient vibrational motion of the diatomic anion was simulated and the vibrational dephasing times for different solvents determined (Banin *et al.*, 1992).

Detailed femtosecond studies of HgI_2 photodissociation in various solvents have also been performed; these studies should be contrasted with the previously mentioned gas-phase studies by Zewail and co-workers (1992). Such studies are useful in learning about how solvents affect the nuclear motion in the transition state and how they affect the coherent vibrational and rotational motion of the fragment products, in this case HgI (Voth and Hochstrasser, 1996). As the initial and final states before and after application of the laser pump pulse are sensitive

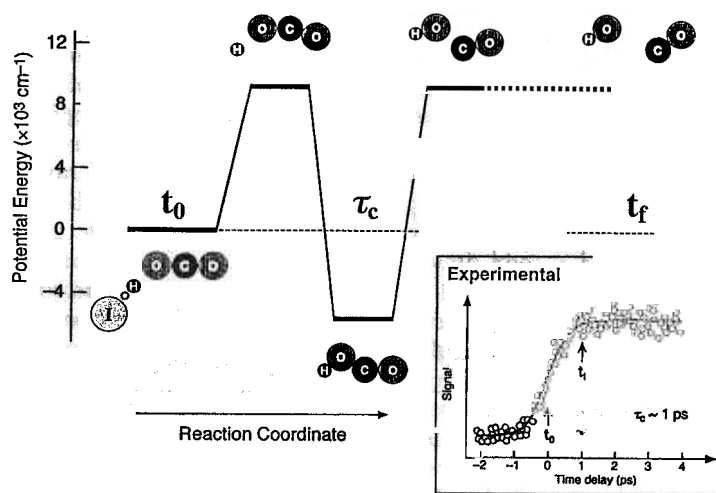


FIG. 19. Femtosecond dynamics of the abstraction reaction $\text{H} + \text{CO}_2 \rightarrow \text{OH} + \text{CO}$ reaction. The potential energy along the reaction coordinate is shown schematically. The experimentally observed rise of the OH from the breakup of the collision complex $[\text{HOCO}]^\ddagger$ is shown with a lifetime $\tau_c \sim 1$ ps. The corresponding structures are noted with emphasis on three snapshots t_0 , τ_c , and t_f (final) at the asymptote region. (Zewail, 1996.)

to the solvent dynamics, the effect of the solvent can be investigated with this femtosecond laser technique.

In Fig. 21 the results of a pump-probe ex-

periment of the photodissociation of HgI_2 in ethanol (Pugliano *et al.*, 1996) are shown. The oscillations in the signal are from the vibration of the HgI photoproduct; the probe

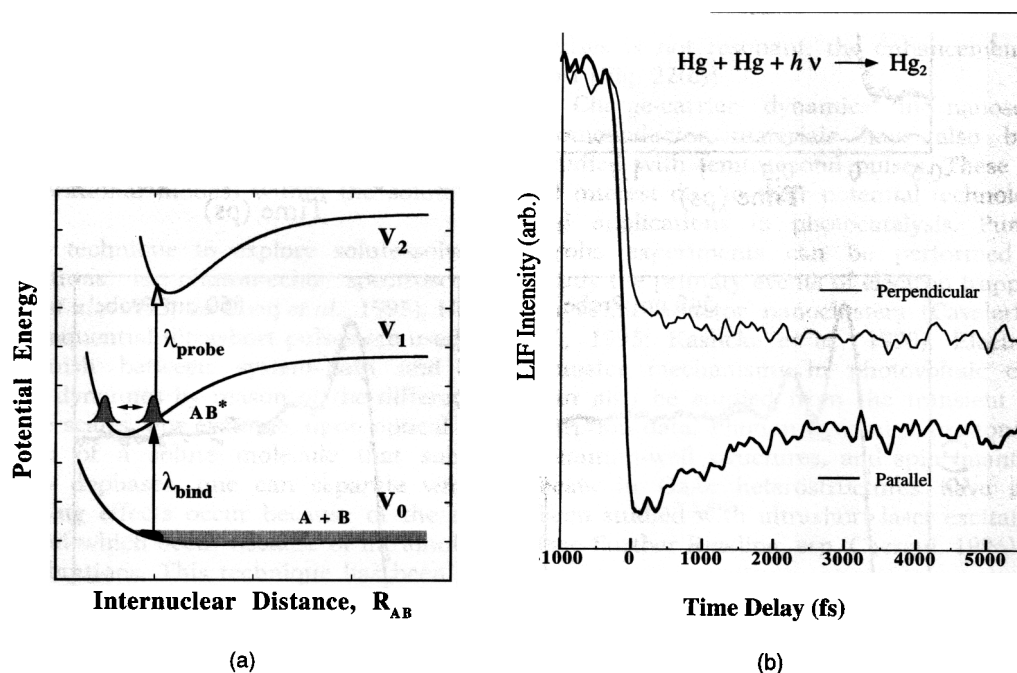


FIG. 20. (a) General scheme for femtosecond photoassociation spectroscopy (FPAS) of a gas-phase system having a repulsive ground state V_0 . Binding by the laser is followed by excitation to a higher state V_2 ; the evolution of the wave packet along V_1 is probed by varying the delay between λ_{bind} and λ_{probe} and monitoring the fluorescence from V_2 or the depletion of the fluorescence from V_1 . (b) FPAS transients showing depletion $D 1_u \rightarrow X 0_g^+$. Data are for the binding and probe lasers polarized parallel or perpendicular to one another. Note the immediate (within the pulse width) formation of photoassociated molecules and the rotational dephasing of the initial anisotropy. (Marvet and Dantus, 1995.)

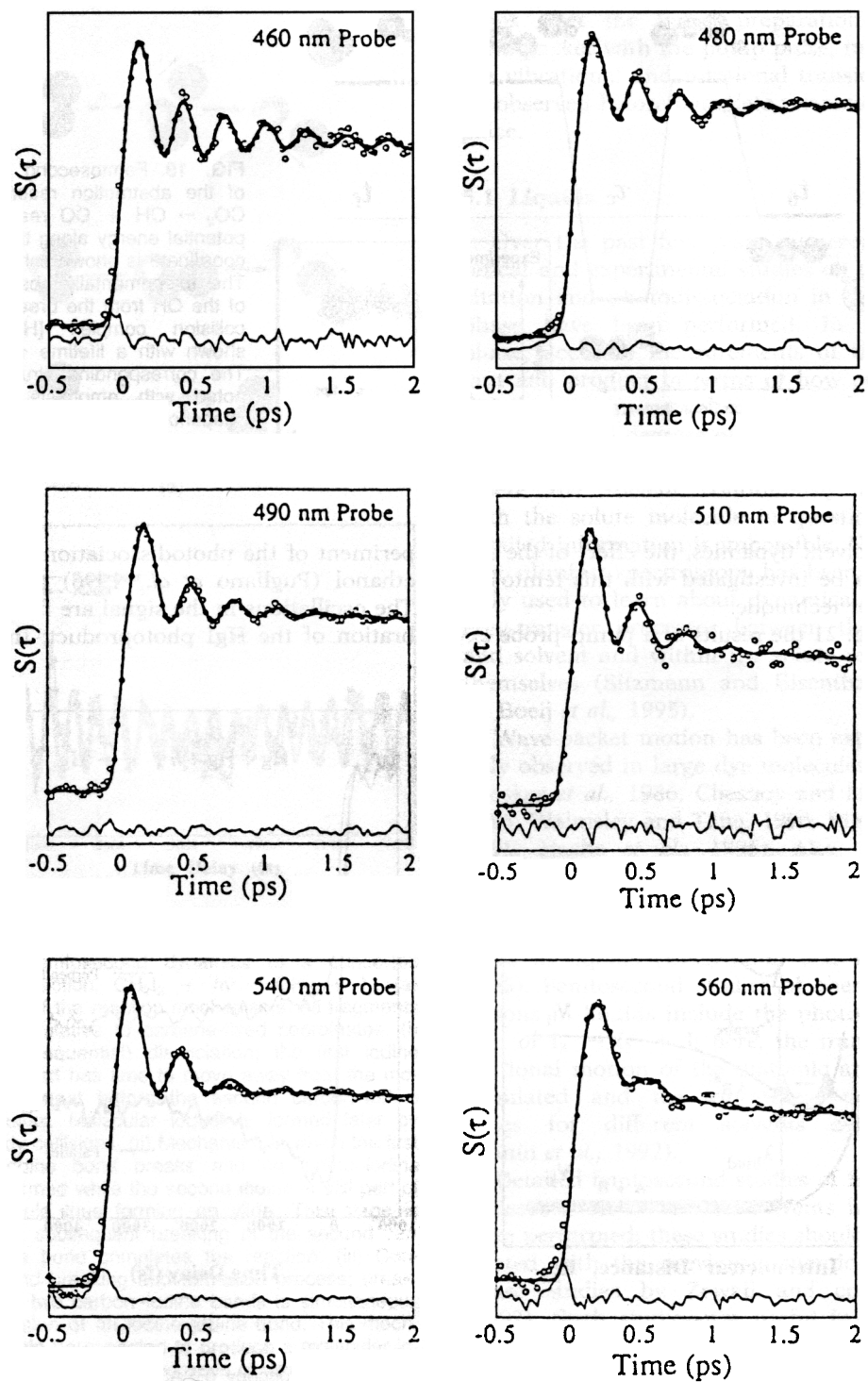


FIG. 21. Magic-angle (relative polarization at 54.7°) pump-probe transients of a 10-mM solution of HgI_2 in ethanol. A pump wavelength of 320 nm was used for each data set. The probe wavelengths between 460 and 560 nm are designated in each of the panels. The open circles are the data points, the bold solid lines are the fits to the molecular response function, and the thin lines are the residuals of the fits. Compare these transients with those shown in Fig. 16 obtained in the gas phase. (Pugliano *et al.*, 1996.)

pulse excites the ground electronic state of HgI to the excited B state. Different probe wavelengths access different regions of the HgI ground potential and therefore monitor different vibrational states of the HgI population. Note that all vibrational transient signals decay on account of the dephasing effects of the solvent. Compare the data in the presence of the solvent (Fig. 21) with the data obtained in the gas phase (Fig. 16).

Another important issue in condensed-phase processes is energy dissipation. The rate of vibrational energy transfer from the excited solute into the solvent-molecule motions can be described as frictional energy loss, and femtosecond studies allow one to measure these relaxation rates. Frictional effects on chemical reactions in the condensed phase such as isomerization of large molecules like stilbene can also be examined. In particular, comparisons of ultrafast studies that monitor the dynamics of stilbene isomerization both as an isolated molecule and in solution can help to elucidate the effect of solvents on intramolecular vibrational redistribution (IVR) within stilbene (Sension *et al.*, 1993). Thus, in addition to measuring the rate of energy transfer from solute to solvent, FTS techniques allow one to study the influence of solute-solvent interaction on energy-transfer dynamics (*i.e.*, between different vibrational modes) within the solute itself.

One technique to explore solute-solvent interactions is photon-echo spectroscopy (Yang *et al.*, 1995; de Boeij *et al.*, 1995). Here three sequential ultrashort pulses are used to distinguish between system-bath and vibronic dynamics by reason of the difference in time scales. For example, upon optical excitation of a solute molecule that subsequently dephases, one can separate which dephasing effects occur because of the solvent and which occur because of intramolecular vibrations. This technique has been exploited in observing dephasing rates of dye molecules in different solvents.

5.2 Solids

Observation of molecular motions in the solid phase has also been achieved with femtosecond pulses. The example chosen to illustrate these observations is the impulsive stimulated Raman scattering (ISRS) of an

organic crystal (α -perylene). The technique involves a sudden (impulse) driving force exerted by a short pulse on a Raman-active vibrational mode of the crystal. The force initiates coherent vibrational oscillations that are monitored by a delayed probe pulse; notice the great similarity with gas- and liquid-phase experiments. Using a train of femtosecond pulses with a time separation that is in resonance with the oscillation of the crystal, Weiner *et al.* show an enhancement of the amplitude of the motion. The data shown in Fig. 22 are the result of excitation with a series of short pulses [Fig. 22(a)] applied to a crystal along a selected lattice coordinate (Weiner *et al.*, 1990). Like someone pushing a child on a swing "on resonance such that the child acquires a small amount of energy with every push," the amplitude of the crystal oscillation is increased. The effect is shown in Fig. 22 where the femtosecond train of pulses sequentially "push" the crystal layers in a certain direction; acquisition of this energy is demonstrated by the increases in the scattering signal [Fig. 22(b) and the simulation, Fig. 22(d)]. When the train of pulses is not resonant, the enhancement is lost [Fig. 22(c)].

Charge-carrier dynamics in nanoscale semiconductor materials have also been studied with femtosecond pulses. These are of interest due to their potential technological applications in photocatalysis. Pump-probe experiments can be performed to study the primary events of electron trapping in semiconductor nanoclusters (Caveleri *et al.*, 1995; Kashcke *et al.*, 1990). Electron-transfer mechanisms in photovoltaic cells can also be studied from the transient absorption data. Phonon dynamics, excitons in quantum-well structures, and spin quantum beats in GaAs heterostructures have also been studied with ultrashort laser excitation (see Further Reading, esp. Chergui, 1996).

5.3 Biological

Femtosecond pulse technology has made inroads in biology as well. Ultrafast processes such as electron transfer in photosynthetic systems can now be studied, including the dynamics of primary events in photobiological systems such as the conversion of solar energy to chemical energy. One of the major goals in these studies is to learn how

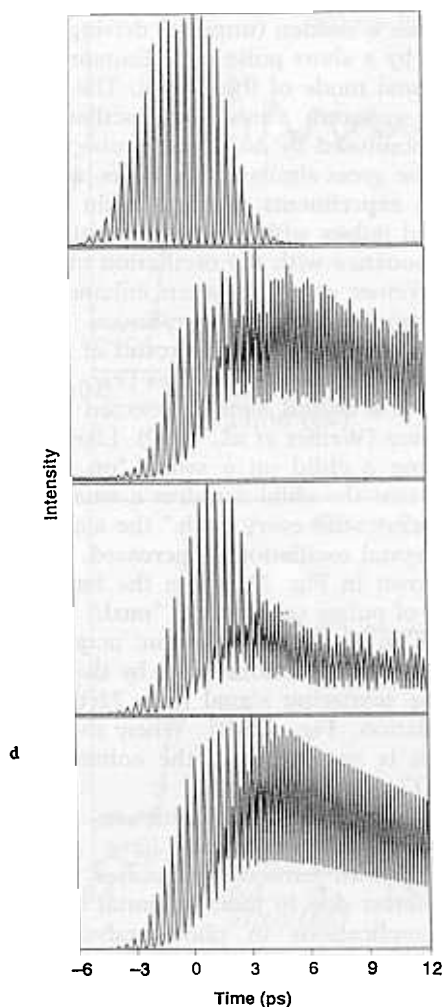


FIG. 22. (a) Cross-correlation measurement of a sequence of femtosecond pulses with a repetition rate of 2.39 THz (419 fs between pulses) produced through pulse-shaping techniques. The pulses can repetitively drive a selected vibrational mode to increase the vibrational amplitude. (b) Impulsive stimulated Raman scattering (ISRS) data from the α -perylene organic molecular crystal driven by a sequence of (*b*-polarized) pulses spaced at 419 fs to match the vibrational period of the 80-cm^{-1} mode. The diffracted signal from the mode grows stronger with each successive pulse, eventually reaching intensity levels comparable to the strongest electronic response. Selective amplification of the 80-cm^{-1} mode is demonstrated. (c) ISRS data from α -perylene driven by a sequence of (*b*-polarized) pulses spaced at 429 fs, slightly off resonance for the 80-cm^{-1} mode. The signal intensity is reduced relative to that in (a), but the vibrational oscillation period is still 419 fs. (d) Simulation of data in (b), assuming a Gaussian temporal profile for the excitation pulse train. In (a) through (d), the zero of time is defined as the center of the input pulse train. (Weiner *et al.*, 1990.)

the energy is distributed, both within the molecule and in the solvent. These studies are an important complement to structural studies of photosynthetic reaction centers, and, in particular, femtosecond studies of the vibrational transients show how the process of electron transfer and vibrational nuclear dynamics are related. Another important process in biological systems is proton transfer. Again, as with electron transfer, this process is strongly dependent on the subpicosecond solute-solvent interactions, which can now be studied with ultrafast pulse techniques.

Other applications of ultrafast spectroscopic techniques to biological molecules include observation of the *cis-trans* photoisomerization of rhodopsin, which has been studied by examining the transient absorption spectra of an excited wave packet created by a 35-fs pump pulse (Wang *et al.*, 1994). Specifically, a pump-probe differential absorption technique was used whereby the 11-*cis* molecule in the S_0 electronic state is pumped up to the S_1 state, where the wave packet can move from its original *cis* configuration to the *trans* configuration whence it decays back to the ground electronic state [Fig. 23(a)]. As shown in the figure, the *cis-trans* conformational change is inhibited by a potential barrier in the S_0 state.

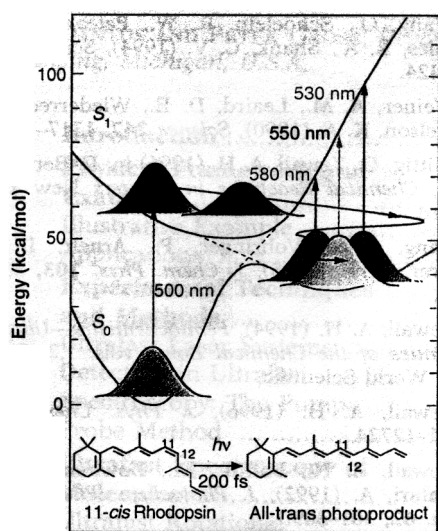
However, as the pumped wave packet is a coherent superposition of vibrational states, this wave packet still oscillates coherently even after decaying to the *trans* conformation in the electronic ground state. These oscillations are detected at various probe wavelengths as shown in Fig. 23(b), which excite the *trans* molecules back up to the S_1 state.

GLOSSARY

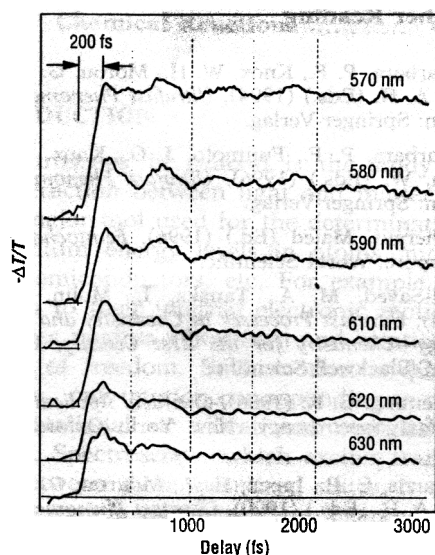
Coherent: This term describes a system having a well-defined phase relationship in its energy states such that the dynamics can be clearly measured.

Dephasing: The process of losing coherence, i.e., becoming incoherent.

Eigenfunction: In general, a mathematical function that is regenerated to within a constant when an operator \mathbf{H} operates on it. Schrödinger's equation, $\mathbf{H}\psi = E\psi$, is an eigenvalue equation where \mathbf{H} is the Hamiltonian.



(a)



(b)

FIG. 23. Ultrafast study of the fundamental steps involved in vision. (a) Schematic potential-energy surfaces for the femtosecond isomerization of rhodopsin after optical excitation of the molecule from the ground state S_0 to the excited state S_1 . The wave packets in the photoproduct potential well illustrate how the ground-state vibrational motion effects the photoproduct absorption. The dashed lines indicate the diabatic pathway along which the reaction proceeds. (b) Differential transient absorption measurements probing the photoproduct absorption after excitation of rhodopsin with a 35-fs pump pulse at 500 nm. Measurements at 620 and 630 nm are multiplied by a factor of 2 for clarity. (Wang *et al.*, 1994.)

nian operator, ψ is the eigenfunction, and E is the eigenvalue (see QUANTUM MECHANICS).

Eigenstate: The wavefunction ψ in Schrödinger's equation represents a characteristic state (hence, "eigen"-state) of the system described by the hamiltonian operator H .

IVR: Abbreviation of "intramolecular vibrational relaxation." A process by which energy deposited in one vibrational mode of a molecule is randomized through the rest of the vibrational modes.

Pump-Probe Method: A technique used in ultrafast spectroscopy based on a pair of laser pulses. The first pulse, the pump, initiates the process of interest, and the second pulse, the probe, monitors the progress as a function of delay time between the pump and probe.

Superposition of States: In quantum mechanics a superposition of states refers to the linear sum of eigenfunctions with a well-defined phase relationship. A superposition of states is time dependent.

Wave Packet: A more or less spatially restricted wave, formed by a superposition of states.

Works Cited

- Backus, S., Peatross, J., Huang, C. P., Murnane, M. M., Kapteyn, H. C. (1995), *Opt. Lett.* **20**, 2000-2002.
- Baltuska, A., Wei, Z., Pshenichnikov, M. S., Wiersma, D. A. (1997), *Opt. Lett.* **22**, 102-104.
- Banin, U., Waldheim, A., Ruhman, S. (1992), *J. Chem. Phys.* **96**, 2416-2419.
- Bigot, J.-Y., Portella, M. T., Schoenlin, R. W., Bardeen, C. J., Migus, A., Shank, C. V. (1991), *Phys. Rev. Lett.* **66**, 1138-1141.
- Bingemann, D., Ernsting, N. P. (1995), *J. Chem. Phys.* **102**, 2691-2700.
- Bowman, R. M., Dantus, M., Zewail, A. H. (1989), *Chem. Phys. Lett.* **161**, 297-302.
- Caveleri, J. J., Colombo, Skinner, D. E., Bowman, R. M. (1995), *J. Chem. Phys.* **103**, 5378-5386.
- Chesnoy, J., Mokhtari, A. (1988), *Phys. Rev. A* **38**, 3566-3576.
- Dantus, M., Rosker, M. J., Zewail, A. H. (1987), *J. Chem. Phys.* **87**, 2395-2397.
- Dantus, M., Bowman, R. M., Grueble, M., Zewail, A. H. (1989), *J. Chem. Phys.* **91**, 7437-7450.
- Dantus, M., Bowman, R. M., Zewail, A. H. (1990), *Nature* **343**, 737-739.
- de Boeij, W. P., Pshenichnikov, M. S., Wiersma, D. A. (1995), *Chem. Phys. Lett.* **247**, 264-270.
- Felker, P. M. (1992), *J. Phys. Chem.* **96**, 7844-7857.

- Felker, P. M., Zewail, A. H. (1987), *J. Chem. Phys.* **86**, 2460–2482.
- Fleming, G. R. (1986), *Chemical Applications of Ultrafast Spectroscopy*, New York: Oxford Univ. Press.
- Fork, R. L., Brito-Cruz, C. H., Becker, P. C., Shank, C. V. (1987), *Opt. Lett.* **12**, 483–486.
- Hashe, T., Ashworth, S. H., Riedle, E., Woener, M., Elsaesser, T. (1995), *Chem. Phys. Lett.* **244**, 164–170.
- Hoffman, G., Oh, D., Chen, Y., Engel, Y. M., Wittig, C. (1990), *Israel J. Chem.* **30**, 115–129.
- Kaschke, M., Ernsting, N. P., Müller, U., Weller, H. (1990), *Chem. Phys. Lett.* **168**, 543–550.
- Lienau, C., Zewail, A. H. (1994), *Chem. Phys. Lett.* **222**, 224–232.
- Lienau, C., Zewail, A. H. (1996), *J. Phys. Chem.* **100**, 18629–18649.
- Lienau, C., Williamson, J. C., Zewail, A. H. (1993), *Chem. Phys. Lett.* **213**, 289–296.
- Liu, Q., Wan, C., Zewail, A. H. (1996), *J. Phys. Chem.* **100**, 18650–18665.
- Manz, J., Wöste, L. (Eds.) (1995), *Femtosecond Chemistry*, New York: VCH.
- Marvet, U., Dantus, M. (1995), *Chem. Phys. Lett.* **245**, 393–399.
- Marvet, U., Dantus, M. (1996), *Chem. Phys. Lett.* **256**, 57–62.
- Materny, A., Lienau, C., Zewail, A. H. (1996), *J. Phys. Chem.* **100**, 18666–18682.
- Pedersen, S., Herek, J. L., Zewail, A. H. (1994), *Science* **266**, 1359–1364.
- Porter, G. (1950), *Proc. R. Soc. London A* **200**, 284–285.
- Pugliano, N., Szarka, A. Z., Hochstrasser, R. M. (1996), *J. Chem. Phys.* **104**, 5062–5079.
- Rose, T. S., Rosker, M. J., Zewail, A. H. (1988), *J. Chem. Phys.* **88**, 6672–6673.
- Rosker, M. J., Wise, F. W., Tang, C. L. (1986), *Phys. Rev. Lett.* **57**, 321–324.
- Rosker, M. J., Dantus, M., Zewail, A. H. (1988), *Science* **241**, 1200–1202.
- Sension, R. J., Repinec, S. T., Szarka, A. Z., Hochstrasser, R. M. (1993), *J. Chem. Phys.* **98**, 6291–6315.
- Sitzmann, E. V., Eienthal, K. B. (1989), *J. Chem. Phys.* **90**, 2831–2832.
- Squier, J., Mourou, G. (1992), *Laser Focus World* (June), 51–60.
- Voth, G. A., Hochstrasser, R. M. (1996), *J. Chem. Phys.* **100**, 13034–13049.
- Walmsley, I. A., Tang, C. L. (1990), *J. Chem. Phys.* **92**, 1568–1574.
- Wang, Q., Schoelein, R. W., Peteanu, L. A., Mathies, R. A., Shank, C. V. (1994), *Science* **266**, 422–424.
- Weiner, A. M., Leaird, D. E., Wiederrecht, G. P., Nelson, K. A. (1990), *Science* **247**, 1317–1319.
- Wittig, C., Zewail, A. H. (1996) in: E. Bernstein, (Ed.), *Chemical Reactions in Clusters* New York: Oxford.
- Yang, T.-S., Vohringer, P., Arnett, D. C., Scherer, N. F. (1995), *J. Chem. Phys.* **103**, 8346–8359.
- Zewail, A. H. (1994), *Femtochemistry—Ultrafast Dynamics of the Chemical Bond*, vols. 1,2, Singapore: World Scientific.
- Zewail, A. H. (1996), *J. Phys. Chem.* **100**, 12701–12724.
- Zewail, A. H., Dantus, M., Bowman, R. M., Mokhtari, A. (1992), *J. Photochem. Photobiol. A: Chem.* **62**, 301–309.
- Zhu, L., Sage, J. T., Champion, P. M. (1994), *Science* **266**, 629–633.

Further Reading

- Barbara, P. F., Knox, W. H., Morou, G. A., Zewail, A. H. (Eds.) (1994), *Ultrafast Phenomena IX*, Berlin: Springer-Verlag.
- Barbara, P. F., Fujimoto, J. G., Knox, W. H., Zinth, W. (Eds.) (1996), *Ultrafast Phenomena X*, Berlin: Springer-Verlag.
- Chergui, Majed (Ed.) (1996), *Femtochemistry*, Singapore: World Scientific.
- El-Sayed, M. A., Tanaka, I., Molin, Y. N. (1994), *Ultrafast Processes in Chemistry and Photochemistry—Chemistry for the 21st Century*, Oxford: IUPAC/Blackwell Scientific.
- Fleming, G. R. (1986), *Chemical Applications of Ultrafast Spectroscopy*, New York: Oxford Univ. Press.
- Harris, C. B., Ippen, E. P., Mourou, G. A., Zewail, A. H. (Eds.) (1990), *Ultrafast Phenomena VII*, Berlin: Springer-Verlag.
- Manz, J., Wöste, L. (Eds.) (1995), *Femtosecond Chemistry*, New York: VCH.
- Martin, J. L., Migus, A., Morou, G. A., Zewail, A. H. (Eds.) (1992), *Ultrafast Phenomena VIII*, Berlin: Springer-Verlag.
- Weirsmas, D. A. (Ed.) (1995), *Femtosecond Chemistry*, Weinheim: VCH.
- Zewail, A. H. (1994), *Femtochemistry—Ultrafast Dynamics of the Chemical Bond*, Vols. 1,2, Singapore: World Scientific.